Selective preparation of collective states in coupled quantum emitters using the SUPER excitation scheme

Johannes Kerber,[1,*] Laurin Ostermann,[1] Vikas Remesh,[2] Helmut Ritsch,[1] and Arpita Pal[1,†]
[1]*Institut für Theoretische Physik, Universität Innsbruck, Technikerstraße 21a, A-6020 Innsbruck, Austria*
[2]*Institut für Experimentalphysik, Universität Innsbruck, Technikerstraße 25d, A-6020 Innsbruck, Austria*

(Received 4 September 2025; accepted 20 January 2026; published 17 February 2026)

The efficient preparation of collective eigenstates of subwavelength-spaced optical dipoles is a prerequisite for observing their signature radiative properties and for their applications in quantum information processing. We theoretically investigate the deterministic preparation of super- and subradiant states of two dipole-coupled two-level quantum emitters at deep-subwavelength separation using the Swing-UP of quantum EmitteR population (SUPER) excitation scheme. Utilizing suitable pulse parameters for two red-detuned, time-overlapping Gaussian pulses, the SUPER scheme enables close-to-unity population inversion in the targeted collective eigenstates. Furthermore, a tunable optical phase in the SUPER scheme enables the simultaneous inversions in both pure super- and subradiant states with finite populations, thereby resulting in the preparation of hybrid collective states. These results are possible to realize with or without an optical cavity. Our approach to populating the collective eigenstates in a cavity environment paves the way for the efficient preparation of these states in the presence of environmental decoherence. Our scheme enables single-photon generation, which is measured using the second-order correlation function. We also discuss in detail possible experimental realizations, in particular using solid-state emitters and molecules.

DOI: 10.1103/fbl4-8j11

I. INTRODUCTION

Collective light-matter interaction among subwavelength-spaced quantum emitters (QEs) is an intriguing research area [1,2] in nonlinear quantum optics. When QEs are positioned sufficiently closely, an individual QE begins to experience the electromagnetic presence of its neighbors through dipole-dipole interaction. This interaction gives rise to collective eigenstates with modified energy levels, entanglement, and distinct radiation properties. Consequently, the QEs' collective emission behavior exhibits superradiance, i.e., enhanced decay, and subradiance, i.e., suppressed decay, compared to the spontaneous emission of a single QE. Historically, following the seminal work of Dicke [3] in 1954, significant research efforts were dedicated to investigating these collective eigenstates [4–13], both theoretically and experimentally, spanning the domain from few [14–19] to many QEs [20–24]. Successful preparation of specific collective eigenstates opens up exciting possibilities, for instance, harnessing the unique radiative properties [10,25–30] and enabling applications in quantum information processing [31,32], storage [22,26], entanglement [33,34], quantum metrology [35,36], and sensing [37].

To observe the characteristic radiative features of these collective states [38–40], in particular when dealing with few emitters, precise experimental control over various factors is typically required. These include tailored internal state selection [41], positioning of the QEs [15,17–19,42], preparing a controlled or near-dissipation-free environment [43,44], and suitable spatial designs to obtain radiative coupling through guided optical modes [18,45]. It is also vital to implement suitable optical control to probe the collective states [15,17–19] and control of optical phases [18,46]. Recent experimental efforts to observe such characteristic radiation properties include studies involving self-assembled solid-state emitters [15], solid-state emitter-photonic crystal waveguide systems [18], molecule-electrode systems [17], molecules embedded as defects in crystals [19], and nanophotonic cavity-QE systems [47].

A key question in this research frontier is how to selectively prepare these collective eigenstates [17,22,47–49], enabling direct access to their distinct radiative features. In this article, we present a theoretical solution by demonstrating that deterministic and efficient population of targeted collective states is indeed possible using the *Swing-UP of quantum EmitteR population* (SUPER) excitation scheme. This fast and pulsed excitation approach effectively penetrates the system's electromagnetic environment, reasonably overcoming the influences of dissipation during the population inversion process. Specific collective eigenstates, in particular dark, bright, as well as hybrid collective states, can be efficiently prepared, as per requirement.

*Contact author: Johannes.Kerber@uibk.ac.at
†Contact author: Arpita.Pal@uibk.ac.at

Published by the American Physical Society under the terms of the Creative Commons Attribution 4.0 International license. Further distribution of this work must maintain attribution to the author(s) and the published article's title, journal citation, and DOI.

SUPER is an off-resonant, yet coherent, two-color pulsed excitation scheme, where a pair of red-detuned, ultrashort Gaussian laser pulses induces an efficient population transfer from an energetically lower to a higher state [50–54], primarily in solid-state emitters. Apart from the fact that it is off resonant, which simplifies the pump laser rejection to a simple spectral filtering, it offers several benefits over conventional resonant excitation methods. For instance, it minimizes decoherence caused by phonons [55] at low temperatures, and has the potential to generate almost ideal single photons reducing possibilities of re-excitation even in the strong coupling regime as well as entangled photon pairs with high concurrence [56] even at elevated temperatures [57] with quantum dot (QD)-cavity systems. Recent studies on the fundamental understanding of the excitation mechanism [58–60] in individual quantum dots offer promising results for intriguing photonic applications.

As a contribution to utilize the SUPER excitation scheme in the realm of collective-light effects, we explore the theoretical possibilities of utilizing the SUPER scheme for the selective preparation of collective eigenstates, in particular, super- and subradiant states. This is achieved in a deep-subwavelength arrangement of two two-level QEs even amidst environmental decoherence. Our proposed theoretical study is not platform specific and relies on a generic two-level QE description. Considering that two decay channels (superradiant and subradiant) emerge with collective states, the SUPER scheme's novelty lies in its ability to access both the short-lived "bright" channel and the long-lived "dark" channel. Our scheme, importantly, allows for the possibility to populate states in both channels to produce hybrid collective states just by controlling the relative optical phases. We provide a detailed theoretical discussion on how so-called mixture weights influence the outcome of a particular excitation process. The efficient preparation of these collective eigenstates offers opportunities to observe their signature dissipative features, in particular with and without a cavity interface [61]. Furthermore, a cavity interface would offer opportunities to analyze photon statistics using the second-order correlation function and reveal signatures of single-photon generation. For completeness, we discuss in detail some realistic experimental possibilities, considering both state-of-the-art and foreseeable developments, involving platforms of solid-state emitters and molecules, to realize our theoretical proposal.

II. THEORETICAL DESCRIPTION

We consider two identical two-level quantum emitters placed at subwavelength separation inside an optical cavity, which is transversely driven via SUPER pulses [see Fig. 1(a)]. The transition frequency and the transition dipole moment of each QE are ω_0 and μ_0, respectively. The spontaneous emission rate is given by Γ. The dipole-dipole interaction Hamiltonian can then be expressed as ($\hbar \equiv 1$)

$$\hat{H}_{\mathrm{DD}} = \sum_i \omega_0 \hat{\sigma}_i^+ \hat{\sigma}_i^- + \sum_{i \neq j} \Omega_{ij} \hat{\sigma}_i^+ \hat{\sigma}_j^-, \tag{1}$$

where the atomic raising operator is defined as $\hat{\sigma}_i^+ = |e\rangle_i\langle g|$ and the lowering operator as $\hat{\sigma}_i^- = (\hat{\sigma}_i^+)^\dagger$. The collective coupling Ω_{ij} is a quantity depending on the interemitter

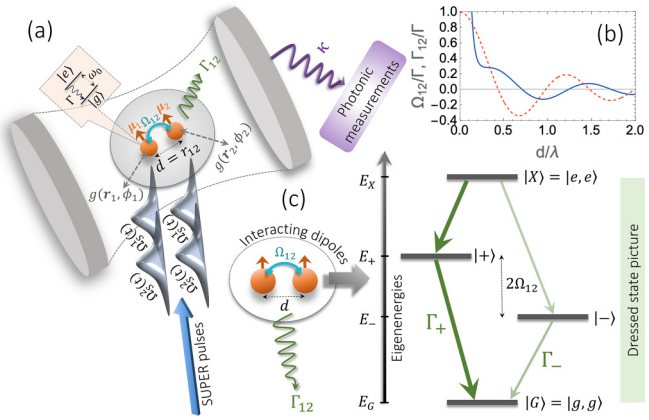


FIG. 1. Schematics for populating collective eigenstates of two interacting dipoles inside an optical cavity with SUPER pulses. (a) Two subwavelength-spaced QE (separation $|\boldsymbol{r}_{12}|$) with dipole moments $\boldsymbol{\mu}_i$ (perpendicular orientations to the separation vector are indicated by orange arrows) are placed inside a single-mode optical cavity of mode frequency ω_c and cavity decay κ. The system is transversely driven by sets of SUPER pulses $[\Omega_S^{I(2)}(t)]$. The inset shows that each QE is a two-level system (ground state $|g\rangle$ and excited state $|e\rangle$) with transition frequency ω_0 (wavelength $\lambda = 2\pi c/\omega_0$, where c is the speed of light) and spontaneous emission rate Γ. The dipole-dipole interaction is mediated by the coherent coupling $\Omega_{12} = \Omega_{21}$ and the decay rates are Γ_{ij} with $i, j \in \{1, 2\}$ (where $\Gamma_{11} = \Gamma_{22} = \Gamma$ and $\Gamma_{12} = \Gamma_{21}$). The atom-cavity coupling for the ith QE is $g(\mathbf{r}_i, \phi_i)$ with $\boldsymbol{r}_i$ the position vector and ϕ_i the relative phase of interaction. The cavity leakage κ allows for photonic measurements in reality. (b) The variation of collective energy shift Ω_{12}/Γ (blue solid line) and collective decay rates Γ_{12}/Γ (red dashed line) for two parallel optical dipoles with interdipole separation $d/\lambda = |\boldsymbol{r}_{12}|/\lambda$. (c) The dressed-state picture of the deep-subwavelength ($d \ll \lambda$) arrangement of two QEs results in eigenstates $\{|G\rangle, |\pm\rangle, |X\rangle\}$ (dressed states) with eigenenergies E_G, $E_\pm$, and E_X, respectively. Modified dissipative decay rates $\Gamma_\pm = \Gamma \pm \Gamma_{12}$ for the cascade transition channels $|X\rangle \Rightarrow |\pm\rangle \Rightarrow |G\rangle$ are displayed.

separation $d = r_{ij} = |\boldsymbol{r}_{ij}| = |\mathbf{r}_i - \mathbf{r}_j|$, its spatial orientation $\hat{\boldsymbol{\varepsilon}}_{\boldsymbol{r}_{ij}} = \boldsymbol{r}_{ij}/r_{ij}$, and dipole orientation $\hat{\boldsymbol{\varepsilon}}_{\boldsymbol{\mu}_{i(j)}} = \boldsymbol{\mu}_{i(j)}/\mu_0$, where $\boldsymbol{r}_{i(j)}$ is the spatial position vector and $\boldsymbol{\mu}_{i(j)}$ the corresponding dipole vector of the $i(j)$th QE with $i, j \in \{1, 2\}$ and $i \neq j$ [see Fig. 1(a)]. For two-level systems, the collective energy shift Ω_{ij} is given by [62]

$$\Omega_{ij} = -\frac{3\Gamma}{4}\Bigg((1-\cos^2\theta)\frac{\cos(k_0 r_{ij})}{k_0 r_{ij}} - (1-3\cos^2\theta)\left(\frac{\sin(k_0 r_{ij})}{(k_0 r_{ij})^2} + \frac{\cos(k_0 r_{ij})}{(k_0 r_{ij})^3}\right)\Bigg), \tag{2}$$

where $k_0 = \omega_0/c$ is the wave number. In this article, we consider that the dipole moment vector of all QEs is aligned perpendicular to the z axis, i.e., $\hat{\boldsymbol{\varepsilon}}_{\boldsymbol{\mu}_i} = \hat{\boldsymbol{\varepsilon}}_{i,\perp_z}$, along which the QEs are positioned and parallel (i.e., H-aggregate configuration [63]). This arrangement leads to $\mathbf{r}_{12} = d \cdot \hat{\boldsymbol{\varepsilon}}_z = -\mathbf{r}_{21}$ and thus $\cos(\theta) = \hat{\boldsymbol{\varepsilon}}_{i,\perp_z} \cdot \hat{\boldsymbol{\varepsilon}}_z = 0$, which simplifies Eq. (2) to the following form:

$$\Omega_{12} = -\frac{3\Gamma}{4}\left(\frac{\cos(k_0 d)}{k_0 d} - \left(\frac{\sin(k_0 d)}{(k_0 d)^2} + \frac{\cos(k_0 d)}{(k_0 d)^3}\right)\right), \tag{3}$$

with $\Omega_{12} = \Omega_{21}$ [see variation in Fig. 1(b)]. The $\hat{H}_{\rm DD}$ [Eq. (1)] can be transformed into the dressed-state basis $\{|G\rangle = |g, g\rangle, |\pm\rangle, |X\rangle = |e, e\rangle\}$ with $|\pm\rangle = 1/\sqrt{2}(|g, e\rangle \pm |e, g\rangle)$ and eigenenergies $E_G = 0$, $E_\pm = \omega_0 \pm \Omega_{12}$, and $E_X = 2\omega_0$ [see Fig. 1(c) and further details are in Appendix A]. In the first excitation manifold, Ω_{12} lifts the degeneracy of the states $|\pm\rangle$. In this manuscript, we will focus our discussions on the symmetric ($|+\rangle$) and the antisymmetric ($|-\rangle$) branch, which illustrates the distance-dependent super- and subradiant channels of the interacting two two-level QEs (see Appendix A for details).

A. SUPER excitation scheme

The SUPER excitation scheme, first proposed theoretically [50] in 2021 and then experimentally demonstrated [51–54], is a rather unconventional scheme for exciting a QE from an energetically lower to a higher state, utilizing a carefully considered combination of two off-resonant Rabi oscillations with frequency modulation or using two far-detuned Gaussian pulses of an approximately picosecond timescale. The Gaussian pulse SUPER scheme is referred to as the two-color SUPER scheme [50]. The pulses overlap in time and result in a beatlike interference. Choosing ideal pulse parameter sets, one can realize a full population inversion to the excited state [50,51,58]. The SUPER pulse can be described as follows:

$$\Omega_{\rm S}(t) = \Omega_{\rm S}^1(t)e^{-i\omega_1 t} + \Omega_{\rm S}^2(t-\tau)e^{-i\omega_2 t + i\varphi_X}, \tag{4}$$

where $\Omega_{\rm S}^i(t) = (\alpha_i/\sqrt{2\pi\sigma_i^2})\exp\{-t^2/(2\sigma_i)^2\}$ with $i \in \{1, 2\}$ are the Gaussian pulses. The pulses are characterized by their pulse area α_i, the temporal FWHM σ_i, detuning $\Delta_i = (\omega_i - \omega_0)$, a temporal shift between the pulses τ and a relative phase φ_X, leading to the SUPER parameter set: $(\Delta_1, \Delta_2, \sigma_1, \sigma_2, \alpha_1, \alpha_2, \tau, \varphi_X)$. In Ref. [50], it was shown that φ_X does not alter the occupation of the final state; therefore, we choose $\varphi_X = 0$ for further discussion, which implies that the parameter set $(\Delta_1, \Delta_2, \sigma_1, \sigma_2, \alpha_1, \alpha_2, \tau)$ will be optimized in later sections to ensure a close-to-unity population inversion in the excited states (collective and noncollective), i.e., $|G\rangle \Rightarrow \{|\pm\rangle, |X\rangle\}$.

B. Two interacting two-level QEs inside an optical cavity

Initially, the system is considered to be in the ground state $|g, g\rangle$. Now the deep-subwavelength QEs experience dipole-dipole interaction $\hat{H}_{\rm DD}$ [Eq. (1)]. We illuminate the system with two identical sets of SUPER pulses consisting of two time-overlapping Gaussian pulses, where each set individually targets one QE, respectively [see Fig. 1(a)]. Exciting each QE with a separate SUPER pulse will allow for a flexible addressing of system states. Further discussions are in Appendix A, Sec. III D, and Appendix B. We consider the system to be inside a single-mode optical cavity to the system [Fig. 1(a)], and we can write the following time-dependent Hamiltonian:

$$\hat{H}_{\rm tot}(t) = \hat{H}_{\rm DD} + \hat{H}_{\rm C} \underbrace{-\frac{1}{2}\sum_i (\Omega_{\rm S}(t)\hat{\sigma}_i^+ e^{i\vartheta_i} + \text{H.c.})}_{\hat{H}_{\rm SUPER}}. \tag{5}$$

Without loss of generality, we set $\vartheta_2 = 0$ and for simplicity we define $\vartheta_1 = \vartheta$ with $\vartheta \in (-\pi, \pi]$, which is the relative optical phase [18,46] (see Sec. VI for details). This allows a straightforward discussion on addressing the two branches (symmetric and antisymmetric) in Fig. 1(c) arbitrarily (see Sec. III D for details). For example, $\vartheta = 0$ selectively couples to the $|+\rangle$ branch while $\vartheta = \pi$ targets the $|-\rangle$ branch. The Hamiltonian for a single-mode optical cavity and the emitter-field coupling is given by

$$\hat{H}_{\rm C} = \omega_c \hat{a}^\dagger \hat{a} + \sum_{i=1}^{2} (g(\mathbf{r}_i, \phi_i)\hat{\sigma}_i^+ \hat{a} + \text{H.c.}), \tag{6}$$

where ω_c denotes the cavity frequency, $\hat{a}^\dagger$ ($\hat{a}$) are the creation (annihilation) operators of the cavity mode, and $g(\mathbf{r}_i, \phi_i) = g(\mathbf{r}_i)\exp(i\phi_i)$ are the distance- and phase-dependent ($\phi_i \in (-\pi, \pi]$) cavity couplings. In a deep-subwavelength arrangement, both QEs experience the same coupling strength, i.e., $|g(\mathbf{r}_1, \phi_1)| = |g(\mathbf{r}_2, \phi_2)| = g \in \mathbb{R}$. Analogous to ϑ_i, the phase factors ϕ_i determine how the cavity mode couples to the system. The phases ϕ_i are induced via backscattering processes in the cavity [64], for instance, due to surface roughness, which results in the coupling of different branches. The relative phase ϑ [Eq. (5)], on the other hand, is an optically (externally) tunable quantity [18,46], in general. Section VI illustrates further details on the interaction phases (ϑ, ϕ_i). As a result, the cavity mode couples purely to the symmetric branch $|+\rangle$ when $\phi_1 = 0 = \phi_2$ and equally couples to both the $|+\rangle$ and $|-\rangle$ branches when $\phi_1 = 0$ and $\phi_2 = \pi/2$. To reduce computational complexity, Eq. (5) is transformed into the rotating frame of ω_1, i.e.,

$$\begin{aligned}\hat{H}(t) =& -\Delta_1 \sum_i \hat{\sigma}_i^+ \hat{\sigma}_i^- + \sum_{i\neq j} \Omega_{ij}\hat{\sigma}_i^+ \hat{\sigma}_j^- \\ & - \Delta_c \hat{a}^\dagger \hat{a} + \sum_i (g(\mathbf{r}_i, \phi_i)\hat{\sigma}_i^+ \hat{a} + \text{H.c.}) \\ & - \frac{\Omega_{\rm S}^1(t)}{2}\sum_i (\hat{\sigma}_i^+ e^{i\vartheta_i} + \text{H.c.}) \\ & - \frac{\Omega_{\rm S}^2(t-\tau)}{2}\sum_i \left(\hat{\sigma}_i^+ e^{i\vartheta_i + i(\Delta_1 - \Delta_2)t} + \text{H.c.}\right),\end{aligned} \tag{7}$$

with $\Delta_c = \omega_c - \omega_1$. Under the Born-Markov approximation, the system's dynamics is governed by the master equation

$$\partial_t \hat{\rho}(t) = -i[\hat{H}(t), \hat{\rho}(t)] + \hat{\mathcal{L}}_{\rm Coll}[\hat{\rho}(t)] + \hat{\mathcal{L}}_{\rm C}[\hat{\rho}(t)], \tag{8}$$

where $\hat{\rho}$ is the density matrix. The collective dissipation of the open quantum system is subject to the following Liouvillian superoperator:

$$\hat{\mathcal{L}}_{\rm Coll}[\hat{\rho}] = \sum_{ij} \frac{\Gamma_{ij}}{2}(2\hat{\sigma}_i^- \hat{\rho}\hat{\sigma}_j^+ - \{\hat{\sigma}_j^+ \hat{\sigma}_i^-, \hat{\rho}\}), \tag{9}$$

where $\{\cdot, \cdot\}$ indicates the anticommutator and Γ_{ij} are the dipole orientation and distance-dependent collective decay

TABLE I. The fixed pulse parameter sets for the ith pulse, where $i = 1, 2$: detuning ($\Delta_{1(2)}$) and FWHM (σ_i) in SI and scaled units (s.u.), respectively.

Units	Δ_1	Δ_2	σ_1	σ_2
SI	-5 meV	-10 meV	6 ps	6 ps
s.u.	-7595.58	$-15\,191.16$	0.006	0.006

rates.The collective decay rates are given by [62]

$$\Gamma_{ij} = \frac{3\Gamma}{2}\left((1-\cos^2\theta)\frac{\sin(k_0 r_{ij})}{k_0 r_{ij}} + (1-3\cos^2\theta)\left(\frac{\cos(k_0 r_{ij})}{(k_0 r_{ij})^2} - \frac{\sin(k_0 r_{ij})}{(k_0 r_{ij})^3}\right)\right), \quad (10)$$

which, for the same dipole orientations as in Eq. (2), simplifies to

$$\Gamma_{12} = \frac{3\Gamma}{2}\left(\frac{\sin(k_0 d)}{k_0 d} + \left(\frac{\cos(k_0 d)}{(k_0 d)^2} - \frac{\sin(k_0 d)}{(k_0 d)^3}\right)\right), \quad (11)$$

with $\Gamma_{12} = \Gamma_{21}$ [see Fig. 1(b) for the variation with d/λ]. Similarly, the cavity loss is accounted for by the following Liouvillian:

$$\hat{\mathcal{L}}_C[\hat{\rho}] = \frac{\kappa}{2}(2\hat{a}\hat{\rho}\hat{a}^\dagger - \{\hat{a}^\dagger\hat{a}, \hat{\rho}\}). \quad (12)$$

This theoretical description of the coupled dipole system, embedded within a cavity and excited by the SUPER scheme, provides an opportunity for fundamental theoretical investigation, as detailed below.

III. SELECTIVE PREPARATION OF THE COLLECTIVE EIGENSTATES USING THE SUPER EXCITATION SCHEME

The SUPER scheme offers many different advantages that conventional excitation schemes fail to provide [50–54,56–58]. First, it is an off-resonant excitation scheme, and therefore, spectral separation of the pumping laser and the resulting emission is, in principle, trivial. This is especially true for spectroscopy of collective states. One of the advantages are nonunique parameter sets (see Sec. II A). For simplicity, since the SUPER parameter set ($\underline{\Delta_1}, \underline{\Delta_2}, \underline{\sigma_1}, \underline{\sigma_2}, \alpha_1, \alpha_2, \tau$) consists of seven adjustable parameters, we choose to fix the underlined parameters. The parameters are provided in SI units and also in dimensionless units (with respect to Γ and λ, where $1/\Gamma = 1$ ns) as detailed in Table I.

The pre-adjusted parameters reduce the full variable space $\mathbb{R}^7$ to $\mathbb{R}^3$. Theoretically, one can choose the fixed parameters arbitrarily; however, the respective quantities should be easily adjustable experimentally. If not specifically mentioned, we set $\Gamma\tau = 0$, thus, we obtain the variable space $\mathbb{R}^2$. In Sec. III A, we set $\Gamma\tau = 0.004$ for achieving near-unity inversion in state $|-\rangle$. Finding two suitable choices for α_1 and α_2 to populate a certain state $|i\rangle \in \{|\pm\rangle, |X\rangle = |e,e\rangle\}$ can be done rather easily by computing the final population as follows:

$$P_i^{\text{end}} = \text{Tr}(|i\rangle\langle i|\hat{\rho}(t_{\text{end}})), \quad (13)$$

where t_{end} denotes the end of pulse duration in the SUPER mechanism.

In the following section, we first investigate the influence of a cavity environment (in Sec. III A) and discuss possible effects of environmental decoherence (in Sec. III B) on the preparation of collective states. Subsequently, we disregard the optical cavity interface and discuss the optimized SUPER parameter sets that lead to close-to-unity population inversions in collective states in Sec. III C. Finally, we study the preparation of hybrid collective states relying on the tunability of relative optical phases (ϑ) in Sec. III D.

A. Population inversion into collective states in an optical cavity

We position our dipole-interacting QEs inside an optical cavity [Fig. 1(a)] where the interaction with the cavity mode [Eq. (7)] can be controlled by adjusting the cavity coupling strength g and the cavity coupling phases ϕ_i ($i \in \{1, 2\}$). The dissipation of the system is governed by the Lindblad master equation [Eq. (8)], when the system is weakly coupled to the environment. In Fig. 2, we demonstrate how the interdipole separation d, the SUPER phase ϑ [18,46], and the cavity coupling phases ϕ_i affect the system's population dynamics. The cavity mode is resonant to the atomic transition frequency, i.e., $\Delta_c = \Delta_1$. We consider the following two cases. In Figs. 2(a)–2(d), we investigate the case of efficiently populating $|+\rangle$ for $d = 0.01\lambda$ (brown gradient sets of lines) and $\phi_1 = 0 = \phi_2$ (here the cavity couples to the $|+\rangle$ branch only). Figures 2(e)–2(h) display the case of efficiently populating $|e,e\rangle$ state at $d = 0.1\lambda$ (blue gradient lines) with $\phi_1 = 0$ and $\phi_2 = \pi/2$ (here the cavity couples to both $|\pm\rangle$ branches equally). We choose $\vartheta = 0$ in Fig. 2, because, on the one hand, we know that for $\vartheta \neq 0$ the SUPER mechanism couples partially (for $\vartheta = \pi$ fully) to the $|-\rangle$ branch, resulting in less population inversion of P_+ in the first case. On the other hand, $\vartheta = 0$ allows for an estimation of excess nonzero P_- population stemming from a close-to-resonant cavity coupling in the second case [Fig. 2(e)].

First, we focus on state preparation. In Figs. 2(a)–2(c), we observe that $P_{e,e}$ (brown/blue curve) remains small after the SUPER excitation, while $P_+ > 91\%$ (brown curve) is achieved for $d = 0.01\lambda$. Increasing the separation to $d = 0.1\lambda$ (blue line) implies a strong decrease of Ω_{12} [Fig. 1(b)] and reduces the energy shift of $|+\rangle$, i.e., $E_+ \approx -\Delta_1$, leading to a decrease of P_+ to $P_+ \ll 25\%$ with zero population in $|-\rangle$. Similarly, in Figs. 2(e)–2(g) we obtain $P_{e,e} > 95\%$ for $d = 0.1\lambda$ (blue line). The population decreases to $P_{e,e} \ll 10\%$ for $d = 0.01\lambda$ (brown line), owing to the fact that the excitation process hinges on a large energy shift E_+ when we use identical individual SUPER pulses for each QE (see Appendix A). We find $P_+ > 60\%$ for $d = 0.01\lambda$ (brown line). The SUPER scheme is designed to invert in between two isolated energy levels. Thus, parameters optimized for a pair of energy levels may work reasonably well for other sets of discrete energy levels too. Note that the decimal-precision pulse parameters utilized here are state-of-the-art numbers (as also in Refs. [50,51,56,58]) and the theoretical optimization process is strongly dependent also on the decimal precisions of the pulse profile (as in Fig. 2), in general. However, total probability, $P_{e,e} + P_+ + P_- + P_G = 1$, must remain conserved. We find $P_- \approx 0$ (brown line) and $P_- > 0$ (blue line). This is

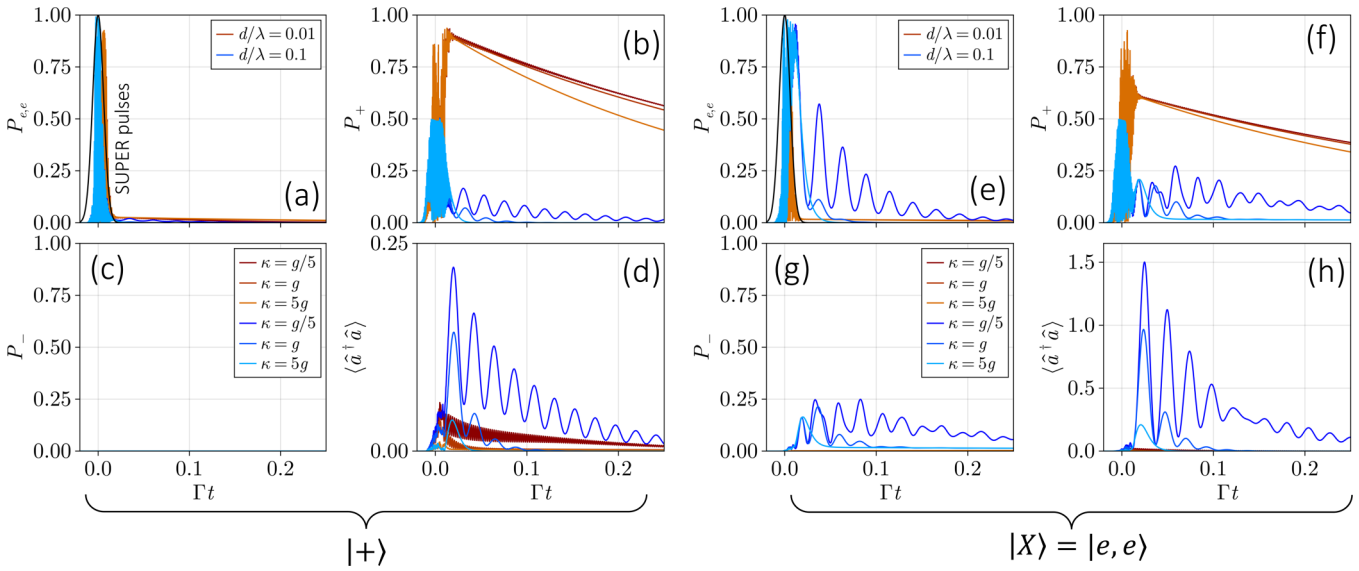


FIG. 2. Population dynamics for interacting subwavelength-spaced two QEs inside an optical cavity. The superradiant state $|+\rangle$ is populated with the SUPER pulses using the pulse areas $\alpha_1 = 68.25\pi$ and $\alpha_2 = 59.05\pi$ [panels (a)–(d), optimized for the highest inversion when $d/\lambda = 0.01$]. We address $|X\rangle = |e,e\rangle$ with $\alpha_1 = 51.74\pi$ and $\alpha_2 = 70.48\pi$ [panels (e)–(h), optimized for the highest inversion $d/\lambda = 0.1$]. In particular, the blue and the brown gradient sets of curves represent $d = 0.1\lambda$ and $d = 0.01\lambda$, respectively. For all curves, the cavity parameters $g = 100\,\Gamma$ and $\kappa \in g\{1/5, 1, 5\}$ are indicated by the respective colors as visualized in panels (c) and (g) for each d value. Panels (a) and (e) show the population of $|X\rangle$, i.e., $P_{e,e}$, together with the overlapping pulse profiles [black/gray lines (overlapping)]. Panels (b) and (f) display the temporal evolution of population of the $|+\rangle$ state (P_+). In panels (c) and (g), the population in $|-\rangle$ (P_-) are shown. The intracavity photon numbers ($\langle \hat{a}^\dagger \hat{a} \rangle$) are displayed in panels (d) and (h).

explained by looking at the cavity coupling. In Figs. 2(a)–2(d), the cavity couples to the $|+\rangle$ branch only. We find an oscillating photon number $\langle \hat{a}^\dagger \hat{a} \rangle$ [Fig. 2(d)] for $d = 0.1\lambda$ (blue line), as with $E_+ \approx -\Delta_1$ the photons couple resonantly to the cavity. This is not the case for $d = 0.01\lambda$, where $E_+ \gg -\Delta_1$. In Figs. 2(e)–2(h); however, here, we observe $P_- > 0$ because the cavity couples to both branches equally. Ideally, we expect a maximal value of two photons in Fig. 2(h) for $d = 0.1\lambda$ due to the decay cascade $|(e,e), 0_\mp, 0_\pm\rangle \Rightarrow |\pm, 1_\mp, 0_\pm\rangle \Rightarrow |(g,g), 1_\mp, 1_\pm\rangle$. However, only $\max_{\Gamma t} \langle \hat{a}^\dagger \hat{a} \rangle = 1.5$ can be achieved, because one photon is emitted earlier, yielding a nonzero probability to re-excite the system: $|\pm, 1_\mp, 0_\pm\rangle \Rightarrow |(e,e), 0_\mp, 0_\pm\rangle$. Although, here we choose $\Delta_c = \Delta_1$, in principle, one could also choose other cavity frequencies; those could result in different temporal evolution of the population of the prepared state, however, the respective maximum achievable population and robustness over different cavity coupling regimes would remain the same.

The swing-up mechanism, considering a single QE [50,51], implies an off-resonant coupling to the cavity during the excitation process [56]. This stems from ac Stark shifts [65] induced by the SUPER pulses. Hence, in Sec. III C, we will neglect the cavity when finding optimal parameters for an efficient inversion of the collective states. In the latter part of this article, cavity interface will be utilized for some photonic measurements.

Note that the phases ϕ_i and ϑ possess an equivalent influence on accessing the bright (superradiant) or dark (subradiant) channel, as we are in the deep-subwavelength regime, for both the cavity and the SUPER coupling. In this section, as we are discussing the effect of the optical cavity, we vary ϕ_1, ϕ_2. In Sec. III D, later, we will explore the possibility of accessing both dark and bright channels by changing only the relative phase ϑ and neglecting the cavity interface.

B. SUPER excitation of coupled quantum emitters amidst decoherence

Let us consider two QEs at deep-subwavelength separation experiencing strong dipole-dipole interaction in a noisy environment. The system is then being illuminated by sets of SUPER pulses to have a near-unity inversion in one of the collective states $|+\rangle$ or $|-\rangle$ [Fig. 1(a)]. Note that the layer of pure electromagnetic interaction, which includes dipole-dipole interaction and corresponding collective decays, is in reality *immersed* in a dissipative environment, which is an "ocean" of many frequencies and experiencing environmental triggers. Hence, the layer experiences finite environmental exchanges [see Fig. 3(a)]. These exchanges include interaction with phonons (lattice vibrations) due to elevated temperature or from the on-site static energy imperfections of the QEs, as well as the influence of dephasing mechanisms via the substrate.

1. Decoherence in an optical cavity

We already know that the SUPER scheme [50,51,58] is a mechanism only between two discrete energy levels (e.g., $|G\rangle \Rightarrow |\pm\rangle$ and $|\pm\rangle \Rightarrow |X\rangle$). Here, we consider SUPER pulses of a duration of $\sigma_i = 6$ ps (Table I). In Ref. [57], it has been shown that the excitation to an energetically higher state for a single quantum dot is only weakly influenced by phonons. This is a remarkable advantage over other coherent excitation schemes, for instance, two-photon absorption, where the achieved final population in the excited state decreases

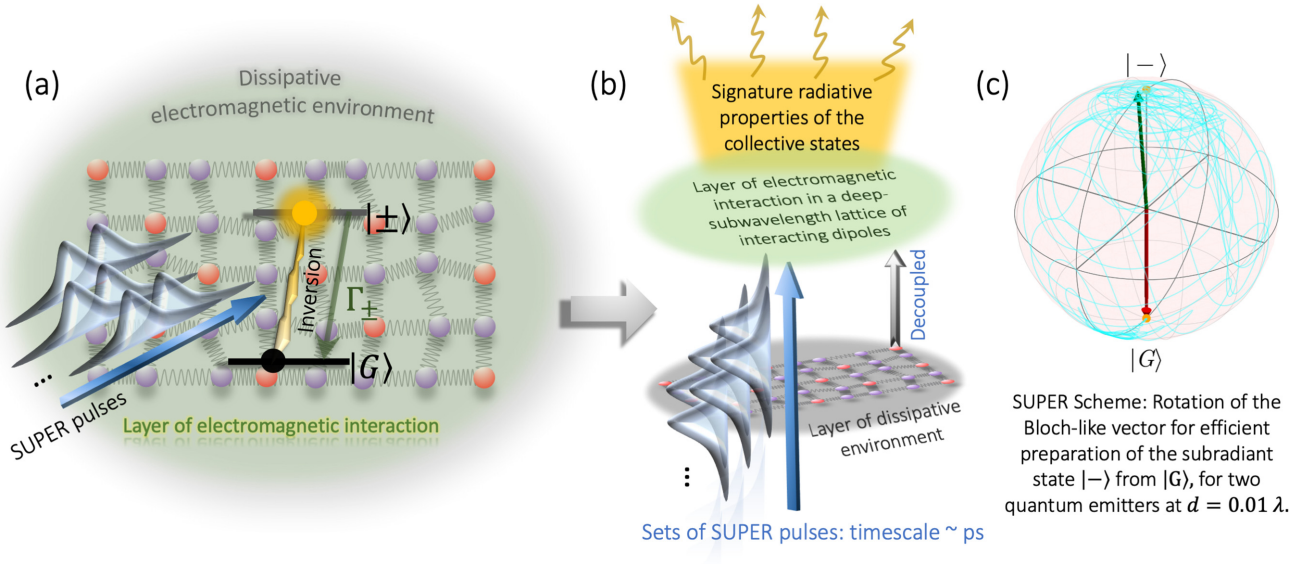


FIG. 3. (a) A schematic illustration of the efficient inversion by ultrashort SUPER pulses (approximately picoseconds) that drive the system from the ground state ($|G\rangle$) (black circle) to one of the collective states ($|\pm\rangle$) (yellow circle) of the QEs, with collective decay rates $\Gamma_{\pm}$. The interacting dipoles form a "layer of electromagnetic interaction" immersed in a dissipative environment, e.g., due to phonons (shown above as lattice vibrations in the background), having a timescale larger than the SUPER process or on-site energy imperfections (symbolically represented by different colors in the background lattice). A near-unity inversion can be accomplished despite the presence of the dissipative environment. (b) SUPER pulses can then selectively and separately (to a reasonable extent) access the pure layer of dipole-dipole interaction, which was earlier submerged into the dissipative environment and open opportunities to directly witness the signature collective radiative properties. (c) Dynamics of the density matrix corresponding to the sub-Hilbert space spanned by $\{|G\rangle, |-\rangle\}$ (see Sec. III D), represented as Bloch-like vector (cyan curve) for the $|G\rangle \Rightarrow |-\rangle$ transition, using the SUPER scheme in the absence of a cavity (pulse parameters are mentioned in the text). The red downward vector denotes the initial state $|G\rangle$, and the green upward vector represents the final $|-\rangle$ state.

rapidly for higher temperatures [57]. Intuitively, the SUPER scheme works fast, relies on off-resonant pulses, and importantly, traces an unconventional trajectory during the rotation of the Bloch vector on the Bloch sphere [50] and thereby induces an effective decoupling of the excitation (target state) from the environment [56,57]. In the coupled emitter case as discussed in Sec. III A, we found a similar suppression of the environmental coupling when populating bright $|+\rangle$ states (at $d = 0.01\lambda$) with SUPER pulses [Fig. 2(b)], which leads to very low population in the cavity mode [brown sets of curves in Fig. 2(d)] in the presence of cavity-mediated system-environment interaction. The excited collective states $|\pm\rangle$ and also $|X\rangle$ experience an ac Stark shift [65], and the respective Bloch-like vector (see Sec. III D) also traces an unconventional time-dependent trajectory on the Bloch sphere. As a result, they become off resonant to the cavity mode, which drastically minimizes the possibility of re-excitation even in the strong system-cavity coupling regime. In short, the environmental exchanges of the pure "layer of electromagnetic interaction" are much reduced in an optical cavity.

2. *Decoherence from static position disorders*

Now, we map the above picture intuitively in the domain where QEs are experiencing position fluctuations in an environment/substrate. In particular, we disregard the cavity and consider the influence of lattice vibration [Fig. 3(a)] as on-site static position disorders (roughly). Here, we consider a small fluctuation in the position of each QEs and the modified Hamiltonian in Eq. (5) can then be rewritten as

$$\hat{\tilde{H}}^{\rm ph}_{\rm tot}(t) = \underbrace{\hat{\tilde{H}}^{\rm ph}_{\rm DD}(\epsilon_r, \tilde{r}_{ij})}_{\substack{\text{modified } \hat{H}_{\rm DD} \\ \text{for on-site} \\ \text{static position disorder}}} - \frac{1}{2}\sum_i (\Omega_{\rm S}(t)\hat{\sigma}_i^{+} e^{i\vartheta_i} + \text{H.c.}). \tag{14}$$

The last term represents the SUPER pulses. For parallel dipoles (in H configuration) [as in Fig. 1(a)], we redefine Eq. (1) as follows:

$$\hat{\tilde{H}}^{\rm ph}_{\rm DD}(\epsilon_r, \tilde{r}_{ij}) = \sum_i \omega_0 \hat{\sigma}_i^{+}\hat{\sigma}_i^{-} + \sum_{i\neq j} \tilde{\Omega}_{ij}(\epsilon_r|\tilde{\mathbf{r}}_{\mathbf{i}} - \tilde{\mathbf{r}}_{\mathbf{j}}|)\hat{\sigma}_i^{+}\hat{\sigma}_j^{-}. \tag{15}$$

Here, $\tilde{\mathbf{r}}_{\mathbf{i}}$ is the mean position of the ith QE (considering a normal distribution with width ϵ_r and averaged over many realizations) and $\tilde{r}_{ij} = |\tilde{\mathbf{r}}_{\mathbf{i}} - \tilde{\mathbf{r}}_{\mathbf{j}}|$ is the modified interemitter separation. In reality, ϵ_r could be roughly realized as a temperature-dependent quantity and a theoretically tunable parameter. We consider that the fluctuations around the position of the QE's are much smaller, i.e., $(|\mathbf{r}_{\mathbf{i}}| - |\tilde{\mathbf{r}}_{\mathbf{i}}|)/|\mathbf{r}_{\mathbf{i}}| \ll 1$. For a deep-subwavelength lattice, i.e., $d = 0.01\lambda$, the collective optical shifts are normally very large in magnitude, hence, one can write

$$\frac{|\Omega_{ij}(|\mathbf{r}_{\mathbf{i}} - \mathbf{r}_{\mathbf{j}}|) - \tilde{\Omega}_{ij}(\epsilon_r|\tilde{\mathbf{r}}_{\mathbf{i}} - \tilde{\mathbf{r}}_{\mathbf{j}}|)|}{|\Omega_{ij}(|\mathbf{r}_{\mathbf{i}} - \mathbf{r}_{\mathbf{j}}|)|} \ll 1. \tag{16}$$

This implies that at low temperature, i.e., with much slower lattice vibrations (on a timescale greater than picoseconds),

one can make the following reasonable approximation:

$$\hat{\tilde{H}}^{\rm ph}_{\rm DD}(\epsilon_r, \tilde{r}_{ij}) \simeq \hat{H}_{\rm DD}(r_{ij}). \tag{17}$$

Therefore, for slower lattice vibrations, the ultrashort SUPER scheme (approximately picoseconds) effectively accesses the pure collective states $|\pm\rangle$ of the interacting QEs [dynamics guided by Eq. (8)] and then induces an ac Stark shift to the energy levels and a rotation of the Bloch-like vector on the Bloch sphere, which effectively decouples the "layer of electromagnetic interaction" from the other modes of the dissipative environment that were near resonant before (following the similar principle as with the resonant cavity case, which we demonstrated earlier in Sec. III B 1) [see Figs. 3(b) and 3(c)]. Subsequently, as the temperature rises, the excitation with the SUPER scheme will not be significantly impacted (in contrast to other coherent excitation methods), as was also demonstrated in Ref. [57] with a single quantum dot-cavity system. However, to be really precise, one needs to take into account the whole spectrum of modes of the reservoir for a specific system. On a hopeful note, even if substantial modes are initially coupled to the pure "layer of electromagnetic interaction," the prepared collective state with SUPER pulses will always help the excitation to become decoupled from some of the modes of the reservoir, and thereby provide access to more robust signature radiation properties.

Figure 3(c) displays the trajectory of the Bloch-like vector (in the absence of a cavity and Sec. III D later illustrates more on it) when addressing $|G\rangle \Rightarrow |-\rangle$ transition with SUPER pulses for two deep-subwavelength QEs. We utilize the parameters from Table I, $d = 0.01\lambda$, $\vartheta = \pi$, $\Gamma\tau = 0.004$, pulse areas $\alpha_1 = 20\pi$ and $\alpha_2 = 40\pi$ to obtain around 99% inversion in the $|-\rangle$ state.

3. Decoherence due to on-site energy imperfection

As discussed in the section above, equivalently, one could also consider the effect of on-site static energy disorder (i.e., nonidentical energy levels) in the QEs [instead of cavity interaction (Sec. III B 1) or position disorder (Sec. III B 2) of the QEs]. This is particularly common for solid-state emitters or molecules when embedded in a substrate. As discussed in Ref. [8], the on-site energy disorders (inhomogeneous broadening) can be accounted for via a modified Hamiltonian [66,67]

$$\hat{\tilde{H}}^{e}_{\rm tot}(t) = \sum_{\nu=1}^{2} \omega^{\rm e}_{\nu} \hat{\sigma}^{+}_{\nu} \hat{\sigma}^{-}_{\nu} + \sum_{i\neq j} \Omega_{ij} \hat{\sigma}^{+}_{i} \hat{\sigma}^{-}_{j} \underbrace{- \frac{1}{2} \sum_{i} (\Omega_{\rm S}(t) \hat{\sigma}^{+}_{i} e^{i\vartheta_i} + {\rm H.c.})}_{\hat{H}_{\rm SUPER}}, \tag{18}$$

where ν represents the site number and $\omega^{\rm e}_{\nu}$ is the site energy, which varies due to the dissipative environment. This could be modeled as an average over many realizations of a normal distribution of width ϵ_e around atomic frequency ω_0; i.e., $\omega^{\rm e}_{\nu} = \epsilon_e \omega_0$. This will also provide an equivalent description of the system-environment interaction as we had utilized earlier with the cavity mode (in Sec. III A).

In Ref. [8], the authors theoretically demonstrated the robustness (up to a reasonable extent) of the effect of energy disorder on superradiance and superabsorption. For very high disorder, the pure bright and dark collective states would start mixing. Thus, for small (reasonable) changes in the site energy, i.e., roughly when

$$\frac{\epsilon_e}{\Gamma} = \frac{\omega^{\rm e}_{\nu}}{\omega_0} \lesssim 1, \tag{19}$$

the Hamiltonian in Eq. (18) will prohibit mixing of pure bright and dark states (see, for instance, Fig. F1 in Ref. [68] in the context of bio-inspired nanoscale ring geometry). The above limit allows for pure collective states to retain their unique optical signatures. With reasonably less disorder, therefore for superradiance, the effective linewidth of the collective states will remain increased ($\Gamma + \Gamma_{12}$), i.e., exhibit faster decay and for subradiance it will remain narrowed down ($\Gamma - \Gamma_{12}$), i.e., showcase lesser decay (of course when compared to the case of independent QE). The prepared states also exhibit robustness against environmental triggers (up to an extent) for the SUPER excitation process (as happens in the presence of the cavity interface). To illustrate once again, following our previous insights, the efficiently prepared collective states will eventually experience an ac Stark shift when prepared by SUPER pulses, and the Bloch-like vector traces an unconventional rotation on the Bloch sphere [similar to Fig. 3(c)], and as a result, become off resonant to the environmental effects (reasonably). The excitation will therefore remain effectively decoupled from the dissipative environment caused by site energy imperfections (up to an extent), which allows for the system to showcase its signature radiative properties [as shown in Fig. 3(b)].

4. Further possibilities

Looking ahead, we expect the qualitative features discussed above might remain the same for very deep subwavelength-spaced lattices of quantum emitters, in particular, molecular arrangements in biological systems [69,70] to investigate more clearly the presence and/or influence of the collective states [71,72] in light harvesting mechanism (although, note that system-environment interaction is unfortunately too complex in this case to explain solely relying with Markovian master equation approach as detailed in Ref. [68]) or synthetic molecular configurations [73] (system-environment interaction is fortunately more controllable here [30]). In these cases, or more generally, using a single set of SUPER pulses (in particular, only two pulses) could be experimentally more feasible for preparing collective states, amidst a reasonable decoherence in the environment. It may also mitigate the effects of environmental dissipation up to a certain extent, allowing one to isolate (reasonably) and study the pure layer of electromagnetic interaction, governed by the dipole-dipole interaction. We intend to address this possibility in the future. In this context, it is worth noting that molecular aggregates are known to be resilient (upto a certain extent) to imperfections, such as inhomogeneous broadening [74] and dephasing [75]. If this were true, this venture to efficiently and selectively prepare collective states with SUPER scheme would be crucial for understanding the importance of the

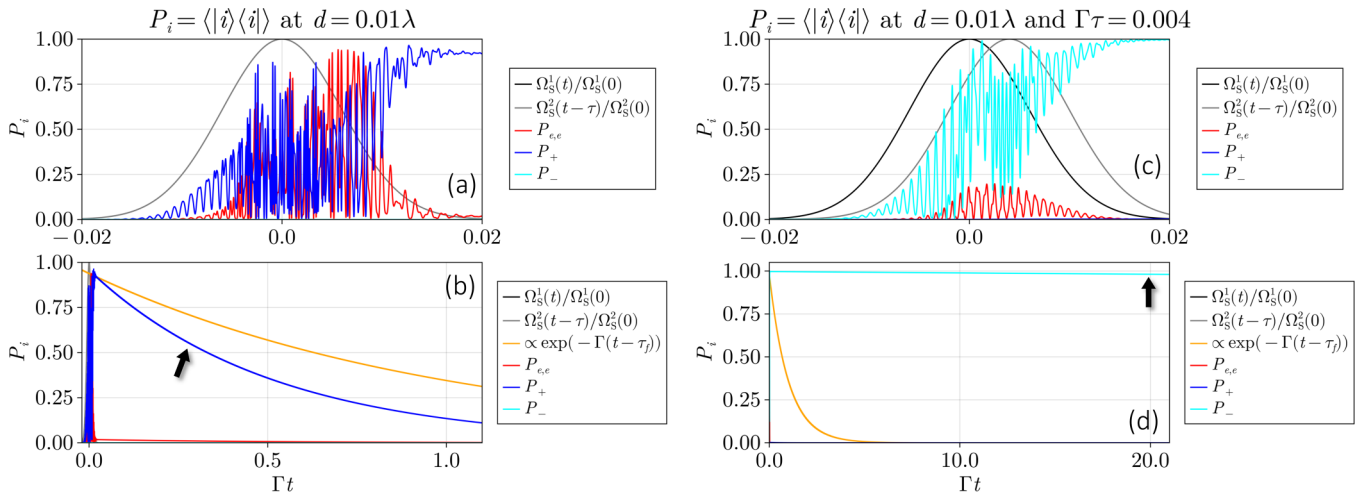


FIG. 4. Efficient preparation of collective eigenstates ($|\pm\rangle$) of deep-wavelength-spaced ($d = 0.01\lambda$) optical dipoles using the SUPER scheme in the absence of an optical cavity. Gaussian pulse profiles $\Omega_S^{1(2)}(t-\tau)/\Omega_S^{1(2)}(0)$ are represented with black (gray) solid curves in panels (a) and (b) (zero time delay, $\Gamma\tau = 0$) and (c) and (d) (finite time delay, $\Gamma\tau = 0.004$). Here, $\Omega_S^{1(2)}(0)$ simply denote the maximal values of the corresponding pulses. In particular, in panels (a) and (b), we address the superradiant $|+\rangle$ state with a SUPER phase $\vartheta = 0$ and pulse areas $\alpha_1 = 68.25\pi$ and $\alpha_2 = 59.05\pi$. A population inversion of $P_+ > 91\%$ in state $|+\rangle$ (blue solid curve) is achieved. In panels (c) and (d), to address the subradiant $|-\rangle$ state, we use $\vartheta = \pi$ and pulse areas $\alpha_1 = 20\pi$ and $\alpha_2 = 40\pi$. This results in a population inversion of $P_- > 99\%$ (cyan solid curve) in state $|-\rangle$ [panels (c) and (d)]. The decay of these prepared super- and subradiant state populations is shown on a longer timescale in panels (b) and (d) and indicated by black arrows. The orange solid line in panels (b) and (d) depicts the independent exponential decay with rate Γ for comparison. The long-time evolution demonstrates a superradiant decay of $|+\rangle$ in panel (b) (blue solid curve) and, importantly, a very long-lasting excitation storage characteristic, i.e., subradiance, for $|-\rangle$ (cyan solid curve) in panel (d).

biological geometry purely relying on quantum optical Hamiltonians for exploring the landscape of bio-inspired optically efficient configurations [8,29,68,76–78]. However, these insights will nevertheless require more detailed and in-depth future investigations for confirmation.

C. Parameters for cavityless inversions in bright and dark collective states

In this section, we discuss and detail the optimized SUPER parameter sets for obtaining a high population inversion in the states $|i\rangle \in \{|\pm\rangle, |X\rangle\}$. We remove the cavity from our model, as the SUPER excitation scheme is robust to the choice of cavity coupling strength (as discussed in Sec. II B). Figures 4(a) and 4(c) show the swing-up behavior without a cavity for efficient preparation of the collective states $|\pm\rangle$ of two-interacting two-level QEs at deep subwavelength separation [Fig. 1(c)], i.e., $d = 0.01\lambda$. With optimal pulse parameters, we can achieve approximately 91% population for the $|+\rangle$ state [Fig. 4(a), blue solid curve] and over 99% for the $|-\rangle$ state [Fig. 4(c), cyan solid curve]. For both cases, the final population in $|X\rangle = |e,e\rangle$ is near zero. We display the long-term dynamics after the selective preparation of the collective states $|\pm\rangle$ as well [Figs. 4(b) and 4(d)]. The bright state (blue solid curve) decays faster [Fig. 4(b)] and the dark state [Fig. 4(d)] (cyan solid curve) decays much slower than the independent decay of the individual QEs (orange dotted curve). It is important to note that the SUPER mechanism, therefore, allows one to access bright and dark states selectively (this is crucial as dark states are, in general, decoupled from the electromagnetic environment) by a suitable choice of externally tunable pulse parameters only. This allows for a direct preparation of a desired collective state. Looking at the existing experimental studies dealing with solid-state emitters and molecules [15,17–19], our above results might motivate approaches to selective preparation of collective states in interacting QE systems.

It is important to note that the SUPER parameter sets are not unique, as displayed in Fig. 5 and also previously demonstrated in literature when dealing with single quantum dots [50,56,57]. This implies that the final probabilities P_+^{end}, P_-^{end} are by no means rigorous upper bounds. In this section, we explicitly write P_i^{end} instead of P_i, pointing out that we focus on the final population immediately after the SUPER procedure. For the present article, we consider $P_+^{\text{end}} > 91\%$ and $P_-^{\text{end}} > 99\%$ to be sufficient. In Fig. 5, we display the heatmaps with optimized parameters of the final population P_+^{end}, P_-^{end} and $P_{e,e}^{\text{end}}$ of $|+\rangle$, $|-\rangle$ and $|e,e\rangle = |X\rangle$ at $d = 0.01\lambda$, respectively (we focus mainly on achieving an as high as possible population inversion for $|\pm\rangle$). We use a 64×64 parameter domain, that is, 64×64 combinations of $\alpha_1 \in [20, 100]$ and $\alpha_2 \in [40, 120]$ for $|+\rangle$ state and of $\alpha_1 \in [20, 80]$ and $\alpha_2 \in [20, 80]$ for $|-\rangle$ state, chosen equidistantly.

Furthermore, the SUPER parameters are highly sensitive to drastic changes of the collective energy shifts Ω_{12} [Eq. (3)] of the levels, which depend on the distance d. Hence, if one were to choose a different subwavelength separation, e.g., $d = 0.1\lambda$, then, Ω_{12} would change and imply a significant decrease in the collective energy shift [see Fig. 1(c)], leading to near degenerate energies $E_\pm = -\Delta_1 \pm \Omega_{12} \sim -\Delta_1$. As a result, one would need to suitably optimize the parameters. It turns out that both $|+\rangle$ and $|-\rangle$ states can no longer be

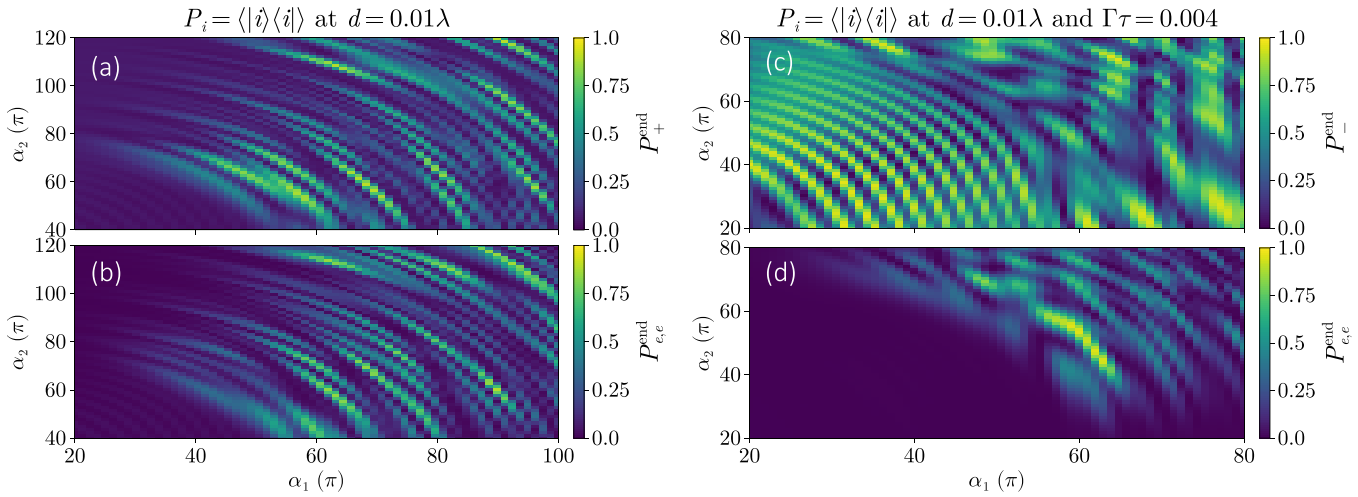


FIG. 5. Heatmaps visualizing pulse parameters $(\alpha_1, \alpha_2, \Gamma\tau)$ for highest possible inversions in state population with $|i\rangle \in \{|+\rangle, |-\rangle, |e,e\rangle\}$ and without the cavity. Parameters $(\Delta_1, \Delta_2, \sigma_1, \sigma_2)$ are fixed (see Table I). For panels (a) and (b), the final populations $P_i^{\mathrm{end}} = \langle |i\rangle\langle i| \rangle$ are plotted for $|i\rangle \in \{|+\rangle, |e,e\rangle\}$ with $\alpha_1 \in [20, 100]$, $\alpha_2 \in [40, 120]$ and $\Gamma\tau = 0$. Bright areas indicate high population inversion. For panels (c) and (d), $P_i^{\mathrm{end}} = \langle |i\rangle\langle i| \rangle$ are depicted for $|i\rangle \in \{|-\rangle, |e,e\rangle\}$ with $\alpha_1 \in [20, 80]$, $\alpha_2 \in [20, 80]$. The $|-\rangle$ branch is successfully addressed using a SUPER phase of $\vartheta = \pi$ and a finite time shift of $\Gamma\tau = 0.004$. In the context of the preparation of collective states, panels (a) and (c) are of primary interest. Note, that we obtain a maximal final population $P_+ = \max_{\alpha_1,\alpha_2} P_+^{\mathrm{end}} > 91\%$ for the parameter set $(\alpha_1 = 68.25\pi, \alpha_2 = 59.05\pi)$ and $P_- = \max_{\alpha_1,\alpha_2} P_-^{\mathrm{end}} > 99\%$ for the parameter set $(\alpha_1 = 20\pi, \alpha_2 = 40\pi)$, as shown in Fig. 4.

populated efficiently when $d \gg 0.01\lambda$ and $\vartheta = 0$ or $\vartheta = \pi$, respectively. Due to the near-degenerate nature of the collective states and duration time of the very short SUPER pulses, populations around $P_\pm^{\mathrm{end}} < 50\%$ can only be achieved.

The above observations for efficient inversions into the respective super- and subradiant states via SUPER pulses are expected to remain qualitatively similar, even with changes in the dipole orientations and in any deep-subwavelength separation of the QEs, as long as the energies $E_\pm$ are approximately the same, i.e., $\Omega_{12}^{\mathrm{mod}} \approx \Omega_{12}$, where $\Omega_{12}^{\mathrm{mod}}$ denotes the energy shift with respect to the modified dipolar orientation and subwavelength separation (the states $|\pm\rangle$ may swap the nature of super- and subradiance, implying $E_\mp^{\mathrm{mod}} \approx E_\pm$). Head-to-tail configuration, i.e., J configuration [63], for instance, where radiative properties will change, may also be addressed with the same parameters (if the above statement is fulfilled).

D. Preparation of hybrid collective states with controlled optical phases

As discussed earlier, both the choice of relative phases in the SUPER scheme (ϑ_i) [Eq. (5)] and in the cavity coupling (ϕ_i) [Eq. (6)] have an equivalent role, allowing for the creation of hybrid collective states tuning phases of the SUPER pulses or the cavity coupling. In this section, we discuss the preparation of collective states, in particular, relying on the relative optical phase ϑ [18,46] for the interacting two two-level QEs. The dressed-state picture (DSP) is discussed in detail in Appendix A. We consider the Hamiltonian in Eq. (A9) and as discussed in Sec. II B, the presence of the optical cavity hardly affects the population inversion to a desired collective eigenstate via the SUPER scheme. Especially, the maximum population is independent of the cavity coupling strength. Hence, we neglect the emitter-cavity coupling for a more concise analysis. The system Hamiltonian in the DSP can now be written as

$$\begin{aligned}\hat{H}_{\mathrm{DSP}}(t;\vartheta) = &\sum_{j\in\{G,\pm,X\}} E_j |j\rangle\langle j| - \frac{1}{2}\sum_{j\in\{\pm\}} (\tilde{\Omega}_{\mathrm{S}}(t)(e^{i\vartheta}(|X\rangle\langle j| \\ &+ \Xi(j)|j\rangle\langle G|) + (\Xi(j)|X\rangle\langle j| \\ &+ |j\rangle\langle G|)) + \mathrm{H.c.}),\end{aligned} \tag{20}$$

where $\tilde{\Omega}_{\mathrm{S}}(t) = \tilde{\Omega}_{\mathrm{S}}^1(t) + \tilde{\Omega}_{\mathrm{S}}^2(t)\exp i(\Delta_1 - \Delta_2)t$, $\Xi(\pm) = \pm 1$, and $\hat{H}_{\mathrm{DSP}}(t;\vartheta)$ is essentially a time t- and phase ϑ-dependent quantity. Considering the orthonormal dressed-states basis: $\mathcal{B}_{\mathrm{DSP}} = \{|G\rangle, |\pm\rangle, |X\rangle\}$, $\hat{H}_{\mathrm{DSP}}(t;\vartheta)$ can be written in matrix representation as

$$\hat{H}_{\mathrm{DSP}}(t;\vartheta) = \begin{pmatrix} E_X & -\frac{\tilde{\Omega}_{\mathrm{S}}(t)}{2}(e^{i\vartheta}+1) & -\frac{\tilde{\Omega}_{\mathrm{S}}(t)}{2}(e^{i\vartheta}-1) & 0 \\ -\frac{\tilde{\Omega}_{\mathrm{S}}^*(t)}{2}(e^{-i\vartheta}+1) & E_+ & 0 & -\frac{\tilde{\Omega}_{\mathrm{S}}(t)}{2}(e^{i\vartheta}+1) \\ -\frac{\tilde{\Omega}_{\mathrm{S}}^*(t)}{2}(e^{-i\vartheta}-1) & 0 & E_- & -\frac{\tilde{\Omega}_{\mathrm{S}}(t)}{2}(-e^{i\vartheta}+1) \\ 0 & -\frac{\tilde{\Omega}_{\mathrm{S}}^*(t)}{2}(e^{-i\vartheta}+1) & -\frac{\tilde{\Omega}_{\mathrm{S}}^*(t)}{2}(-e^{-i\vartheta}+1) & E_G \end{pmatrix}. \tag{21}$$

The above Eq. (21) provides further insights about the system, in particular, the interaction between the dressed states and the SUPER pulses. One finds some nonzero off-diagonal terms depending on ϑ, where $\vartheta \in (-\pi, \pi]$. Since

TABLE II. Mixture weights of $(\hat{H}_{\mathrm{DSP}}(t;\vartheta))_{i,j} = h_{i,j}$ for different ϑ, where $\{i,j\} \in \mathcal{B}_{\mathrm{DSP}}$.

ϑ	$h_{X,+}$	$h_{X,-}$	$h_{+,G}$	$h_{-,G}$
0	$-\tilde{\Omega}_{\mathrm{S}}(t)$	0	$-\tilde{\Omega}_{\mathrm{S}}(t)$	0
$\frac{\pi}{2}$	$-\frac{\tilde{\Omega}_{\mathrm{S}}(t)}{2}(i+1)$	$-\frac{\tilde{\Omega}_{\mathrm{S}}(t)}{2}(i-1)$	$-\frac{\tilde{\Omega}_{\mathrm{S}}(t)}{2}(i+1)$	$-\frac{\tilde{\Omega}_{\mathrm{S}}(t)}{2}(-i+1)$
π	0	$\tilde{\Omega}_{\mathrm{S}}(t)$	0	$-\tilde{\Omega}_{\mathrm{S}}(t)$

these terms quantify the degree of mixture between the $|+\rangle$ and $|-\rangle$ channel, we refer to said terms as *mixture weights*. In Table II below, we explicitly write down the mixture weights for certain choices of ϑ.

The dynamics of $\hat{H}_{\mathrm{DSP}}(t;\vartheta)$ [Eq. (21)] are governed by the master equation [Eq. (8)]:

$$\partial_t \hat{\rho}_{\mathrm{DSP}}(t;\vartheta) = -i[\hat{H}_{\mathrm{DSP}}(t;\vartheta), \quad \hat{\rho}_{\mathrm{DSP}}(t;\vartheta)] + \hat{\mathcal{L}}_{\mathrm{Coll}}[\hat{\rho}_{\mathrm{DSP}}(t;\vartheta)], \tag{22}$$

where we have neglected the cavity. Since $\hat{\rho}_{\mathrm{DSP}}(t;\vartheta)$ acts on the DSP Hilbert space $\mathcal{H}_{\mathrm{DSP}} \cong \mathbb{C}^2 \otimes \mathbb{C}^2$, a Bloch sphere description [79] of the problem is not possible. However, we only want to visualize the energy distribution in the system indirectly; therefore, a subspace-projection procedure using the density matrix $\hat{\rho}$ is sufficient. We rewrite the density matrix as

$$\hat{\rho} = \sum_{i,j\in\{G,\pm,X\}} \rho_{i,j}|i\rangle\langle j|, \tag{23}$$

where $\hat{\rho} = \hat{\rho}_{\mathrm{DSP}}(t;\vartheta)$ and $\rho_{i,j} := \langle i|\hat{\rho}|j\rangle$. We continue by considering only the two-level system: $|G\rangle$ & $|j\rangle$ with $|j\rangle \in \mathcal{B}_{\mathrm{DSP}} \setminus \{|G\rangle\}$ and introduce the projectors $\hat{\Pi}_j = |G\rangle\langle G| + |j\rangle\langle j|$. We obtain the subdensity matrix

$$\hat{\rho}^j_{\mathrm{sub}} = \hat{\Pi}_j \hat{\rho} \hat{\Pi}_j = \begin{pmatrix} \rho_{j,j} & \rho_{j,G} \\ \rho_{G,j} & \rho_{G,G} \end{pmatrix}. \tag{24}$$

We use $\hat{\rho}_{\mathrm{sub}}$ for a Bloch-like interpretation of the dynamics. We do not normalize $\hat{\rho}_{\mathrm{sub}}$, which implies the shortening of the Bloch-like vector (from now on referred to as Bloch vector) is not only caused by decoherence, but also by population reduction of $|j\rangle$, i.e., the origin of the Bloch-like sphere expresses that no population in the $|G\rangle$-$|j\rangle$ subspace is present. We define the Bloch vector as

$$\mathbf{a}_j = \begin{pmatrix} 2\mathrm{Re}\left[\left(\hat{\rho}^j_{\mathrm{sub}}\right)_{G,j}\right] \\ 2\mathrm{Im}\left[\left(\hat{\rho}^j_{\mathrm{sub}}\right)_{G,j}\right] \\ \left(\hat{\rho}^j_{\mathrm{sub}}\right)_{j,j} - \left(\hat{\rho}^j_{\mathrm{sub}}\right)_{G,G} \end{pmatrix}. \tag{25}$$

We apply $\mathbf{a}_j$ for the findings in Fig. 4(a), i.e., for addressing $|+\rangle$ we choose the optimized SUPER pulse areas $\alpha_1 = 68.25\pi$ and $\alpha_2 = 59.05\pi$. Utilizing the optimization procedure, we can find $\alpha_1 = 51.74\pi$ and $\alpha_2 = 70.48\pi$ to target $|X\rangle = |e,e\rangle$ efficiently [Figs. 2(e)–2(h)]. We determine the $\mathbf{a}_j$ dynamics here as well. In both cases, we consider $\vartheta \in \{0, \pi/2, \pi\}$. The Bloch vector trajectories are shown in Fig. 6. Figures 6(a)–6(c) demonstrate that, when targeting the $|+\rangle$ state, the choice of ϑ is crucial. A high population inversion can be observed for $\vartheta = 0$ [in Fig. 6(a)] with some final oscillations around the north pole, i.e., around $|+\rangle$ (blue line). Red chaotic trajectories are present as well; however, note that these contributions never reach a stable vector combination in the vicinity of the $|X\rangle$ north pole. Indeed, the final point (triangle) is located in the vicinity of the sphere's origin. This is expected, because most of the population is present in the $|+\rangle$-$|G\rangle$ subspace close to $|+\rangle$ after the SUPER dynamics, meaning only a small $|G\rangle$ contribution remains in the $|X\rangle$-$|G\rangle$ subspace. Similarly for $|-\rangle$. In this case, the cyan-colored (to target state $|-\rangle$) contributions are insignificantly oscillating as a straight line between the sphere's origin (population leaves $|-\rangle$-$|G\rangle$ subspace) and the ground state $|G\rangle$, that is, as discussed earlier, the "dark" channel can not be populated. The same logic is valid for the panels (b)–(f). The scenario changes when $\vartheta = \pi/2$ [Fig. 6(b)] and the contributions of the "dark" channel become dominant when $\vartheta = \pi$ [Fig. 6(c)]. Hence, in Fig. 6(c) the blue trajectories are now insiginificant, leaving red and cyan to be dominant. However, the

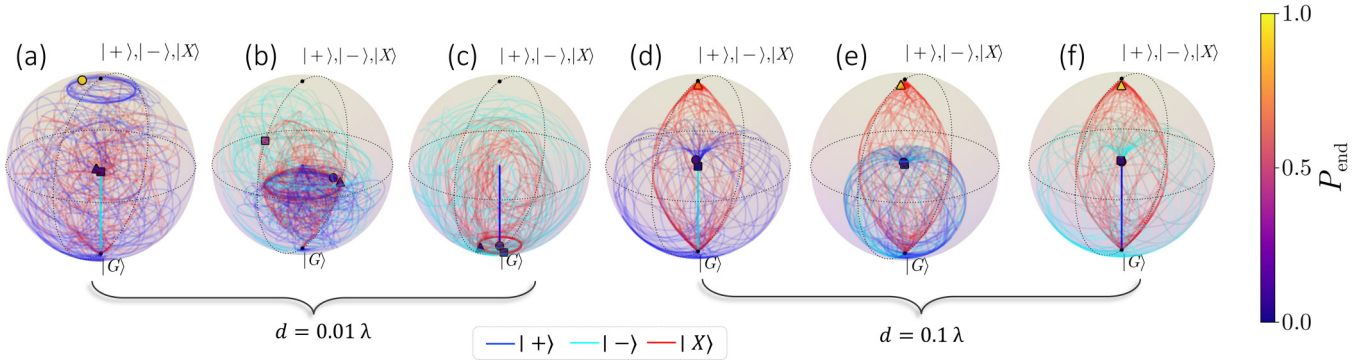


FIG. 6. In panels (a)–(f), blue trajectories on the Bloch spheres represent the population of the superradiant $|+\rangle$ state excited from $|G\rangle$ over time, i.e., P_+ with the relative phase $\vartheta \in \{0, \pi/2, \pi\}$. Similarly, the red trajectories on the Bloch spheres correspond to the time evolution when populating the $|X\rangle$ state, i.e., $P_{e,e}$. The dynamics of the $|-\rangle$ population upon excitation from $|G\rangle$ is represented by cyan trajectories. In panels (a)–(c), the target state $|+\rangle$ is being considered ($d/\lambda = 0.01$), where ϑ is chosen as $\{(a),(b),(c)\} \mapsto \{0, \pi/2, \pi\}$. In panels (d)–(f), the target state $|e,e\rangle$ ($d/\lambda = 0.1$) is visualized. Here, we chose ϑ as $\{(d),(e),(f)\} \mapsto \{0, \pi/2, \pi\}$. Parameters are mentioned in the text. In each panel, the final populations (P_{end}) after the SUPER process on the blue, cyan, and red trajectories are marked with solid colored circle, rectangle, and triangle (vertical color bar is at the right), respectively.

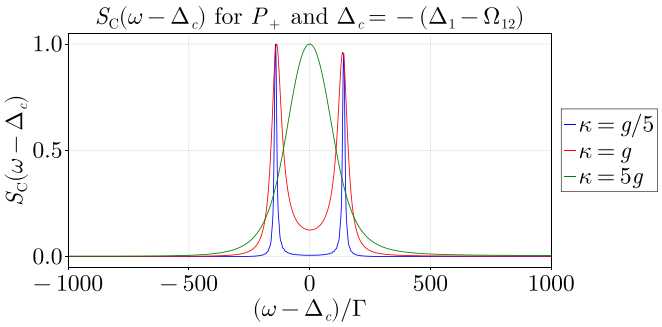


FIG. 7. Normalized cavity emission spectrum for an efficiently prepared "bright" state. The interacting QE-cavity system is prepared in the $|+\rangle$ state with SUPER parameters ($\alpha_1 = 68.25\pi, \alpha_2 = 59.05\pi, \Gamma\tau = 0.0$); however, in contrast to Figs. 2(a)–2(d), we choose $\Delta_c = -(\Delta_1 - \Omega_{12})$, allowing the observation of interesting system dynamics. The spectrum calculation is performed until a time when the system has fully relaxed into the ground state, i.e., $\Gamma t \in [0, \Gamma(T - t_0) = 0.6]$. The cavity decay rates are $\kappa \in g\{1/5, 1, 5\}$ with $g = 100\Gamma$.

collective frequency shift Ω_{12} is large for $d/\lambda = 0.01$ [Fig. 1(b)]. Therefore, due to the large energy gap in the dressed levels [Fig. 1(c)], the SUPER parameter sets are not adjusted to ensure high-population inversion for the energy shift $E_+ = -\Delta_1 + \Omega_{12} \to E_- = -\Delta_1 - \Omega_{12}$. Thus, a large final population P_+ in $|+\rangle$ does not imply a large population P_- in $|-\rangle$. This is consistent with the above discussions considering the different choices for populating $|\pm\rangle$ and $|X\rangle$. The opposite is the case for $|-\rangle$. However, Figs. 6(d)–6(f) show that the above argument is not valid for populating $|X\rangle$ at $d/\lambda = 0.1$. The choice of ϑ decides over the contribution of each channel only; however, since the final energy $E_X = -2\Delta_1$ never changes and $E_+ \approx E_- \approx -\Delta_1$, the end result is always the same final population $P_{e,e} = P_X$. In Appendix B, we provide further details on the influence of ϑ on the populations of the $|\pm\rangle$, $|X\rangle$ states.

In the following sections, we will consider the cavity interface once again to calculate a few observables for easier photonic measurements in reality.

IV. CAVITY EMISSION SPECTRUM

The SUPER excitation process is time dependent. The cavity emission spectrum [56,80] can be calculated using

$$S_C(\omega) = \lim_{T\to\infty} \int_0^T dt \int_0^{T-t} d\tau_t e^{-i\omega\tau_t} \langle \hat{a}^\dagger(t)\hat{a}(t+\tau_t)\rangle, \quad (26)$$

where the t in τ_t reminds us that $\tau_t \in [0, T - t]$ with the upper limit T, is chosen such that the system has fully decayed back to the ground state. We consider the case when the superradiant state ($|+\rangle$) for $d = 0.01\lambda$ is targeted [as also in Fig. 2(b)]. In Eq. (26), we have already substituted $T \to T' = T - t_0 = 0.6\,\Gamma$, where t_0 is the initial time of the SUPER mechanism to avoid numerical artifacts. Figure 7 displays the normalized spectrum $S_C(\omega) \to (S_C(\omega))' = S_C(\omega)/\max_\omega S_C(\omega)$ when efficiently preparing $|+\rangle$ from a strong to weak coupling, i.e., $\kappa \in g\{1/5, 1, 5\}$ via the SUPER scheme. The cavity mode is resonant to the target state $|+\rangle$, i.e., $\Delta_c = -(\Delta_1 - \Omega_{12})$ and couples to the $|+\rangle$ branch only ($\phi_1 = 0 = \phi_2$). In case of $\kappa = g/5$, Fig. 7 shows two characteristic peaks at shifted frequencies $(\omega - \Delta_c) = \pm 141.11\Gamma$. Increasing κ to $\kappa = g$ shifts the peaks slightly toward zero, providing the characteristic frequencies $(\omega - \Delta_c) = \pm 136.91\Gamma$. In the case of a lossy cavity, i.e., $\kappa = 5g$, we obtain peak at $(\omega - \Delta_c) \approx 0.0\Gamma$.

One can expect similar features in the emission spectrum when efficiently preparing the dark $|-\rangle$ state, with suitable pulse parameters [as used in Figs. 4(c)–4(d)] and cavity frequency $\Delta_c = -(\Delta_1 + \Omega_{12})$; however, as the subradiant state decays very slowly [as shown in Fig. 4(d)], T needs to be chosen very large. Therefore, Eq. (26) is numerically expensive and its demonstration is beyond our scope here. When considering hybrid collective states, one could expect similar features. Yet, the choice of the target state will influence the choice of phases (ϑ, ϕ_i) as well as the choice of Δ_c significantly, which are crucial contributors in the optimization process for near-unity inversion with the SUPER scheme.

Since the emission spectrum with SUPER pulses essentially provides the signature of the cavity mode frequencies, as the targeted levels are experiencing ac Stark shifts, the feature of Fig. 7 will be similar for other choices of emitter separations d if the cavity mode is close to resonance with the dressed state transition frequency (as in this case) for a suitable choice of pulse parameters. This may also apply to different dipole orientations of QEs. It seems that $S_C(\omega)$ is an energy-level insensitive observable if SUPER pulses are targeting the excitation.

V. PHOTON STATISTICS

To understand the photon statistics of the emitted light from the cavity, we compute the photon-photon correlation in terms of the second-order correlation function for the cavity mode $g_C^{(2)}(\tau_f, \tau_t)$, immediately after the preparation of the collective states via the SUPER excitation scheme. Here, $\Gamma\tau_f = 0.02$ indicates the end of the pulses, and the pulses are centered around $\Gamma t = 0$. The two-time second-order correlation function has the following form:

$$g_C^{(2)}(\tau_f, \tau_t) = \frac{\langle \hat{a}^\dagger(\tau_f)\hat{a}^\dagger(\tau_f+\tau_t)\hat{a}(\tau_f+\tau_t)\hat{a}(\tau_f)\rangle}{\langle \hat{a}^\dagger(\tau_f)\hat{a}(\tau_f)\rangle\langle \hat{a}^\dagger(\tau_f+\tau_t)\hat{a}(\tau_f+\tau_t)\rangle}. \quad (27)$$

It measures the probability of detecting a second photon at time τ_t, after the first photon is detected at time τ_f. For antibunched nonclassical light, one expects $0 \leqslant g_C^{(2)}(\tau_f, \tau_t) < 1$. In Fig. 8, we plot the variation of $g_C^{(2)}(\tau_f, \tau_t)$ over the scaled time $\Gamma\tau_t$ after the selective preparation of the $|+\rangle$

TABLE III. Exact values of $g_C^{(2)}(\tau_f, 0)$, i.e., immediately after the preparation of target states $|j\rangle$ ($j \in \{\pm, X\}$) via SUPER excitation scheme at different system-cavity coupling regimes $\kappa \in \{g/5, g, 5g\}$.

$\lvert j\rangle$	$\kappa = g/5$	$\kappa = g$	$\kappa = 5g$
$\lvert+\rangle$	1.20×10^{-2}	6.02×10^{-3}	1.68×10^{-4}
$\lvert-\rangle$	3.49×10^{-5}	1.05×10^{-5}	1.22×10^{-6}
$\lvert X\rangle$	0.65×10^{0}	0.62×10^{0}	0.63×10^{0}

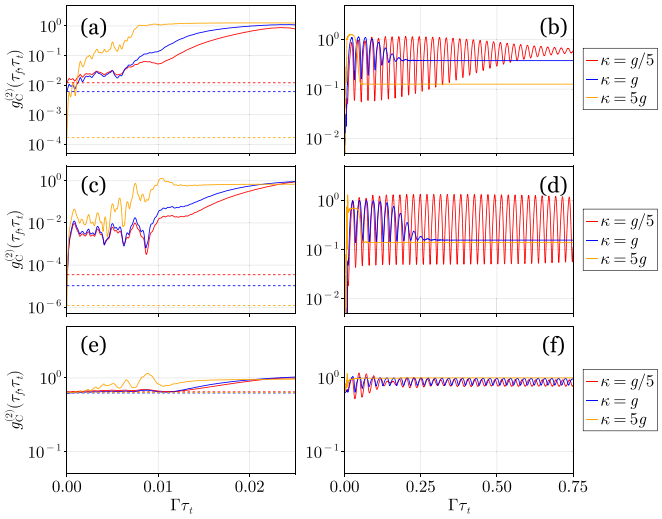


FIG. 8. Intensity correlation function $g_C^{(2)}(\tau_f, \tau_t)$ for $\tau_f = 0.02\,\Gamma$ and with a variable time delay τ_t, after the preparation of the different target states via the SUPER scheme. Different rows in the panels above correspond to signatures after the selective preparation of different target states. The left column [panels (a), (c), and (d)] displays the short-term and the right column [panels (b), (d), and (f)] shows the long-term variations. In particular, $g_C^{(2)}(\tau_f, \tau_t)$ with time delay τ_t are visualized when populating the $|+\rangle$ state [panels (a) and (b)], $|-\rangle$ state [panels (c) and (d)], and $|X\rangle = |e, e\rangle$ state [panels (e) and (f)]. For panels (a)–(d), the QEs are at deep-subwavelength separation ($d = 0.01\lambda$) and for panels (e)–(f) the separation is $d = 0.1\lambda$. The pulse parameters are mentioned in the text. The horizontal dashed lines (red, blue, and orange) in panels (a), (c), and (e) refer to $g_C^{(2)}(\tau_f, 0)$ for the respective coupling regimes (strong, intermediate, and weak), with their values indicated in Table III.

state with $\Delta_c = -(\Delta_1 - \Omega_{12})$ [short time (panel a) and long time (panel b)], the $|-\rangle$ state with $\Delta_c = -(\Delta_1 + \Omega_{12})$ [short time (panel c) and long time (panel d)], and the $|X\rangle = |e, e\rangle$ state with $\Delta_c = -\Delta_1$ [short time (panel e) and long time (panel f)] from a strong to weak cavity coupling regime, i.e., $\kappa \in g\{1/5, 1, 5\}$. The corresponding optimized pulse areas together with the time shift are $(\alpha_1, \alpha_2, \Gamma\tau) = (68.25\pi, 59.05\pi, 0.0)$ for target state $|+\rangle$, $(20\pi, 40\pi, 0.004)$ for state $|-\rangle$, and $(51.74\pi, 70.48\pi, 0.0)$ for state $|X\rangle$, respectively. In addition, for panels (a), (b), (e), and (f), $\vartheta = \phi_1 = \phi_2 = 0$, and panels (c) and (d) require $\vartheta = \pi$, $\phi_1 = 0$, and $\phi_2 = \pi$. In Table III, we explicitly note the numerical values of $g_C^{(2)}(\tau_f, 0)$ for three different coupling regimes and for the respective target states.

In Figs. 8(a), 8(c), and 8(e), we observe $g_C^{(2)}(\tau_f, 0) < 1$, implying a single-photon signature, similar to the case of the SUPER excitation scheme addressing single quantum dots [50,56]. The excitation process by SUPER induces an ac Stark shift for the target states; therefore, the cavity mode remains off resonant during the SUPER excitation process. As a result, the system exhibits single-photon emission at $\Gamma\tau_t = 0$. At long times, we find the existence of antibunched light for all three coupling regimes (Fig. 8). In Figs. 8(b) and 8(d), similar antibunched photon emission can be observed. For $\kappa = g/5$ (red lines), strong oscillations occur, which imply system-photon finite interaction within the cavity. Increasing κ (blue/orange lines) seems to result in damped oscillations, where the system-photon interaction experiences a large reduction. In Fig. 8(e), we can find oscillations of $g_C^{(2)}(\tau_f, \tau_t)$ around unity, implying small nonclassical contributions at finite τ_t for $\kappa \in \{g/5, g\}$. For $\kappa = 5g$, we observe $g_C^{(2)}(\tau_f, \tau_t) \approx 1$.

In Fig. 2(b) (brown curves for $d = 0.01\lambda$), the maximum population is robust to the change of cavity coupling parameter; however, note that the dissipative temporal behavior depends on the choice of (κ, Δ_c). Larger values of κ and off-detuned Δ_c from the target level [as in Fig. 2(b)] result in a smooth population decay, in contrast to small κ and resonant Δ_c to the target level (more strong coupling to the environment), which yield oscillatory decay. A consequence of off-resonant Δ_c is that the cavity mode has a very small number of photons [brown curves line in Fig. 2(d)] for all coupling regimes. In Table III, we find the lowest $g_C^{(2)}(\tau_f, 0)$ at $\kappa = g$ (1.68×10^{-4}) when $|+\rangle$ is just prepared. This could indicate an approach in the photon domain toward ideal single-photon states [$g_C^{(2)}(\tau_f, 0) = 0$] or even quantum non-Gaussian states [81,82], i.e., conceptually, those subsets of nonclassical states lie deep below [$g_C^{(2)}(\tau_f, 0) \ll 1$] the conventional nonclassical limit [83]. In the strong-coupling regime, $g_C^{(2)}(\tau_f, 0)$ is still low $\sim 10^{-2}$, which indicates that the targeted level $|+\rangle$ is reasonably well decoupled from the environment. However, at weak coupling $\kappa = 5g$, we find $g_C^{(2)}(\tau_f, 0) = 1.68 \times 10^{-4} \ll 1$, indicating that environmental decoupling of the target state is much more prominent (as expected). For populating the $|-\rangle$ state, similar features can be observed [see Figs. 8(c) and 8(d)], as this case is also governed by the same fundamental physical principles. At $\kappa = 5g$, the lowest $g_C^{(2)}(\tau_f, 0) = 1.22 \times 10^{-6}$, even lower than for the previous case. Note, $|-\rangle$ is already substantially decoupled from the environment due to its subradiant nature. When prepared efficiently, under the illumination by SUPER, the pulses induce ac Stark shifts, more decoupling from the environment and prohibiting re-excitation results in $g_C^{(2)}(\tau_f, 0) = 3.49 \times 10^{-5} \ll 1$ (see Table III), even in the strong system-cavity coupling regime (much lower than the case for state $|+\rangle$). In short, the second-order correlation function provides the same insights as the population dynamics (Fig. 2) demonstrated earlier. As discussed in Sec. III B, other environmental triggers, such as position fluctuations and energy imperfections (upto a reasonable extent), are expected to reflect similar features in $g_C^{(2)}(\tau_f, 0)$ for a deep-subwavelength arrangement.

At $\tau_t = 0$, we obtain $g_C^{(2)}(\tau_f, 0) < 1$ for the case of targeting $|X\rangle$ (see Table III, the exact values and features are the same as discussed above), showing initially antibunched light. In Fig. 2(h), we obtain a finite population in the cavity (blue curve, largest value ~ 1.5); hence, the cavity is in this case coupled resonantly to the dipole system. We obtain a small $g_C^{(2)}(\tau_f, 0)$, but not as small as for earlier cases. In Fig. 8(f), we encounter a numerical instability at longer times (in particular, shortly after $\Gamma\tau_t = 0.1$ due to low-mode photon numbers), which we counteracted by scaling the numerator and denominator of $g_C^{(2)}(\tau_f, \tau_t)$ appropriately on top of the simulated outcomes and obtain $g_C^{(2)}(\tau_f, \tau_t) \sim 1$, at long time as displayed in Fig. 8(f).

VI. POSSIBILITIES FOR EXPERIMENTAL REALIZATION

We now consider a few possible experimental strategies to realize the theoretical proposal described here. Several solid-state quantum emitter platforms may be considered for this purpose. Epitaxial semiconductor quantum dots offer linewidths (best values reported around 700 MHz), high quantum efficiency, and stable emission characteristics. Typical size distributions of these systems are around 10–70 nm in diameter and 1–10 nm in height. The widely used Stranski-Krastanov growth technique and droplet epitaxy techniques, however, result in randomly grown QDs [84]. One could utilize a densely grown QD ensemble and perform statistical analysis of QD distributions to identify pairs that are closely located. Yet this is a time-consuming method and not a scalable one. Site-controlled QDs can be realized through vapor-liquid-solid epitaxy, where nanowire structures are grown in a bottom-up process at predetermined locations, in which QDs are embedded during the growth process. This configuration aligns the QD along the optical axis of the nanowire waveguide, and also facilitates vertical stacking of multiple QDs at separations as low as a few nm [42,85,86]. Another approach of interest may be the pick-and-place method, which enables the transfer of a precharacterized QD from one surface location to another with submicrometer accuracy [87]. Despite its time-consuming nature, arranging high-quality QDs in desired patterns is feasible. Although colloidal QDs offer unique advantages such as solution processability, size tunability, and high-level scalability, their linewidths and coherence properties are potential concerns for our applications. Yet materials such as lead halide perovskite nanocrystals [88] may offer potential alternatives here, with reported linewidths at cryogenic temperatures as low as a few meV [89]. To arrange such solution-processed QDs in desired patterns with unprecedented accuracy, at separations as low as a few nm, DNA origami may be employed [90,91]. With this method, one can expect precise tuning of dipole-dipole interactions to enhance or suppress collective effects. Two-dimensional materials, particularly transition metal dichalcogenides like MoS_2, WS_2, and WSe_2, are another promising platform to implement our proposal, due to their unique optoelectronic properties [92,93]. Quantum emitters in these systems are created via localized strain engineering, using either arrays of nanopillars or nanoholes in the underlying substrate [94]. By using electron beam lithography to define the substrate topography, emitter separations can be controlled up to a few nm. Synthetic chromophore arrangements [73] may also be a platform to realize extremely small intermolecule separation. Finally, organic molecules are also possible material platforms to engineer collective effects [17,19]. They offer much narrower linewidths (around 40 MHz), and are smaller in size, providing significant advantages compared to all the platforms discussed so far. The most popular organic molecules for quantum optics research have been embedded in crystalline hosts such as anthracene or para-terphenyl crystals. While challenges remain, the progress in nanofabrication and engineering suggests that achieving controlled positioning at subwavelength separations is a promising possibility in the foreseeable future. Concurrently, embedding quantum emitters in photonic cavities such as photonic crystal cavities [18,95–97], and compensating the energetic disorder [18] together with tuning mechanisms such as electric [98,99], strain [43,100,101], magnetic field [102,103], temperature [97], or even laser-induced strain [104], one can engineer collective effects with better control.

Coming to the experimental implementation of the proposed scheme, multiple approaches are possible. In Ref. [51], the authors employed a broadband femtosecond laser pulse coupled to a frequency-domain $4f$ pulse shaper to amplitude-shape two desired frequency bands at desired detunings from the target state. On the other hand, in Ref. [54], the authors used two different laser sources tuned to the desired detunings that are temporally synchronized (a necessary condition for the SUPER scheme). In practical terms, both of the schemes have their own advantages and disadvantages. While the pulse-shaping technique needs only a single laser source and thereby reduces the resource overhead, the two-laser technique might be advantageous to circumvent the power limitations due to lossy shaping components such as gratings and spatial light modulators. Furthermore, the pulse-shaping technique intrinsically provides temporally overlapped pulses, while the two-laser technique requires additional temporal synchronization electronics. While the pulse-shaping technique might be bulky, it is highly flexible and customizable for carving different pulse widths and detunings. On the other hand, the two-laser method is limited in flexibility, depending on the initial specifications (i.e., tuning range, pulse width, etc.). The pulse-shaping technique typically employs a diffraction grating to spread the colours in space, which then gets mapped to the Fourier plane using a focusing element like a lens or a concave mirror. At the Fourier plane, an active modulating element like a spatial light modulator or digital micromirror device can be mounted, which can selectively turn on and off the pixels, enabling intensity control of individual pulses and their specific frequency. Considering the parameter range described in Table I, for a QD system emitting around 780 nm, the two required pulses at $\Delta_1 = -5$ meV and $\Delta_2 = -10$ meV detunings with pulse durations around 6 ps with the specified power can be straightforwardly implemented by tuning a broadband 170 fs laser source tuned to 782 nm (which has a total spectral bandwidth of around 15 nm, i.e., 30 meV range). The required power may be independently adjusted by a proper choice of amplitude mask. The versatility of the pulse-shaping technique also allows carving arbitrary amplitude profiles for the individual pulses (i.e., Gaussian, rectangular, etc.). To generate two identical sets [Fig. 1(a)], the simplest method is perhaps to use a Michelson interferometer associated with the pulse shaper. The generated photons can be filtered via narrow band notch filters, etalons, or spatial filtering techniques.

Our scheme for preparing a specific collective state of two interacting, deep-subwavelength-spaced QEs relies, in particular, on the relative phase ϑ when addressing individual QEs with two separate sets of SUPER pulses, as illustrated in Fig. 1(a). This relative driving phase ϑ of pulsed collective excitation can be varied by tuning laser polarization with respect to dipole orientation, as detailed in Refs. [18,46]

for waveguide QED. Consequently, we expect that viable equivalent experimental techniques and on top, if necessary, further suitable engineering to improve the optical addressing of QEs (in particular, drawing inspirations from other platforms: such as, driving induced adjustable near-field phase methods as in use for superconducting qubits in waveguide [16], on-chip circuit QED [105]), could facilitate the realization of our proposed outcomes in the future. To explore the full landscape of the scheme with the optical cavity, we also theoretically consider a phase ϕ_i in the emitter-cavity couplings. This phase can induce effects similar to the relative phase ϑ, as discussed earlier and may arise from nonideal cavity designs, such as backscattering-induced imperfections [64]. Furthermore, the presence of higher-order transverse cavity modes could also serve as a resourceful element in this context. Alternatively, in an ideal cavity, i.e., illumination with a standing wave laser, such effects could be mimicked by the careful placement of QEs (for instance, with respect to the cavity mode function) to induce specific changes in the emitter-cavity couplings, thereby (reasonably) enabling the selective preparation of collective states.

As previously discussed, the SUPER excitation scheme is an optimization process that depends strongly on experimentally controllable parameters such as pulse profiles and laser detunings. Typically, one can identify wide range of these parameters that enable high population inversion in a target collective state, as illustrated by the heatmaps in Fig. 5. Consequently, the SUPER scheme accommodates a broad set of viable parameter choices, including values that donot require fine decimal-level tuning. The experimental realization of the SUPER scheme in a single QD, as reported in Ref. [51], entails that the required precision in both detuning and pulse profile is well within experimental capabilities, indicating that parameter sensitivity is not a limiting factor. Theoretical studies, such as in Refs. [50,56,58], also support this. Moreover, modern commercial lasers exhibit reasonable stability, with fluctuations typically below 0.5%; such variations expected to have a negligible impact on the practical realization of our scheme.

For theoretical demonstration, we have used an optical cavity with system-cavity coupling parameter $g \simeq 65.8\,\mu\text{eV}$ [106] and a cavity decay rate, κ. Such coupling strengths are achievable in principle by using high-quality factor photonic cavities such as photonic crystal waveguides, or ring resonators. The decay rate is defined as $\kappa \in g\{1/5, 1, 5\}$ to indicate the strong, intermediate, and weak coupling regimes, respectively. It is worth noting that the choice of g is flexible; perhaps that would indicate for choosing a suitable optical cavity interface in reality. A smaller g would likely have a minimal impact on the optimized pulse parameters for inversion into collective states via SUPER, and the maximum population may not be significantly affected. However, normally a weakly coupled cavity would offer better single-photon signature (see Sec. V for details), as also noted in single QD-cavity case in Ref. [56]. To measure emission spectrum and photon correlations, one typically uses a high-resolution spectrometer and superconducting nanowire single-photon detector modules compounded with timing electronics. State-of-the-art spectrometers allow for spectral resolution on the order of 0.01 nm (few tens of μeV) and photon counting modules provide time resolution close to 10 ps and efficiencies above 90%.

VII. CONCLUSIONS AND OUTLOOK

In this paper, utilizing a Markovian master equation approach, we have theoretically demonstrated that the selective preparation of the collective states of two deep-subwavelength-spaced, dipole-coupled two-level QEs is possible using the SUPER excitation scheme. This unconventional excitation scheme, with optimized pulse parameters, facilitates the deterministic preparation of the excitation into *bright* as well as very *dark* collective states in the presence of a dissipative environment. Our investigation shows that the ac Stark shift, imparted by the ultrashort, off-resonant SUPER pulses, on the target collective states helps to decouple the excitation from near-resonant environmental modes. This was also previously observed for single QD cases [50,56]. This fundamental physical principle is crucial for improving access to collective states (to a reasonable extent) by mitigating environmental decoherence factors, especially when compared to other coherent excitation schemes [56,57]. This, in turn, provides the first opportunity (theoretical) to directly observe the signature radiative properties of superradiance and subradiance, in QDs and molecules. Our results on the preparation of hybrid super- and subradiant states with controlled optical phases [18,46] may also provide scope for a noninvasive way to produce states equivalent to mixed collective states with atomic disorders [107] and/or spin-phonon hybrid collective state [108]. The detailed discussion on the possible experimental platforms in particular with solid-state emitters and molecules, together with realistic assessments of the feasibility of our scheme, suggests that our theoretical predictions are very likely to be realized.

It is important to note that a reasonably controlled system-reservoir interaction could help to confirm our theoretical estimations. The optical cavity interface first allows us to witness the robustness of collective state preparation with SUPER excitation. It then provides opportunities to intuitively expand our observations to include environmental decoherence originating from static position disorder and inhomogeneous broadening. Our scheme also offers scope to witness a single-photon source [109,110], which would be useful for applications in quantum information processing [31,32]; for instance, in quantum network nodes [111], quantum repeaters [112], and quantum communication and computing [113]. Our findings suggest that this robustness on the generation of single photons from collective states is possible even in the presence of a certain degree of environmental decoherence, potentially making the scheme viable at elevated temperatures, as studied in a single QD-cavity system [57]. This could be a promising development for creating single-photon sources that utilize collective states of interacting QEs and can operate at room temperature [114]. In the context of recent developments in photonic quantum information technologies [115], this would to be a pertinent question to address. Future experimental confirmation of the preparation or presence of collective states in biological light-harvesting complexes [69,70] using the SUPER excitation

scheme could provide more enlightening answers about the validity and applicability of our theoretical interacting dipole model in biological geometries [68]. These outcomes could contribute to new horizons in the evolving landscape of bio-inspired energy-efficient configurations [30,68,76–78].

ACKNOWLEDGMENTS

We thank Gabriela Militani, Charlie Evagora, and René Schwarz for fruitful discussions. This research was funded in whole or in part by the Austrian Science Fund (FWF) 10.55776/ESP682. We also acknowledge the funding from the Austrian Science Fund (FWF) Project No. 10.55776/FG5 (Forschungsgruppe FG 5), 10.55776/COE1 (quantA), and 10.55776/TAI556 (DarkEneT).

DATA AVAILABILITY

The simulations in this manuscript were performed using the QuantumOptics.jl [116], CollectiveSpins.jl [117], and QuantumToolbox.jl [118] frameworks in the JULIA programming language. The panels were prepared using the JULIA framework library [119]. The data that support the findings of this manuscript are openly available [120].

APPENDIX A: DRESSED-STATE PICTURE OF TWO INTERACTING QUANTUM EMITTERS INSIDE AN OPTICAL CAVITY

The bare-basis definition of the Hamiltonian $\hat{H}(t)$ in Eq. (7) is chosen such that the SUPER scheme and the cavity mode can arbitrarily couple to the eigenstates of the dipole-dipole Hamiltonian $\hat{H}_{\rm DD}$. To gain more insight into the system, such as defining collective super- or subradiance, we introduce the dressed-states picture [see Fig. 1(c)]. We begin by reconsidering Eq. (1), in the rotating frame of ω_1 as following:

$$\hat{H}_{\rm DD} = -\Delta_1(\hat{\sigma}_1^+\hat{\sigma}_1^- + \hat{\sigma}_2^+\hat{\sigma}_2^-) + \Omega_{12}(\hat{\sigma}_1^+\hat{\sigma}_2^- + \hat{\sigma}_1^-\hat{\sigma}_1^+), \tag{A1}$$

where $\Omega_{12} = \Omega_{21}$. We can write Eq. (A1) in matrix representation:

$$\hat{H}_{\rm DD} = \begin{pmatrix} -2\Delta_1 & 0 & 0 & 0 \\ 0 & -\Delta_1 & \Omega_{12} & 0 \\ 0 & \Omega_{12} & -\Delta_1 & 0 \\ 0 & 0 & 0 & 0 \end{pmatrix}. \tag{A2}$$

As mentioned in Sec. II, the eigenstates are

$$\begin{aligned} |G\rangle &= |g,g\rangle, \\ |\pm\rangle &= \frac{1}{\sqrt{2}}(|g,e\rangle \pm |e,g\rangle), \\ |X\rangle &= |e,e\rangle, \end{aligned} \tag{A3}$$

which we refer to as dressed states. The corresponding eigenenergies are $E_G = 0$, $E_\pm = -\Delta_1 \pm \Omega_{12}$, and $E_X = -2\Delta_1$. Note that being a distance- and dipole orientation-dependent quantity, the coherent coupling Ω_{12} lifts the energy degeneracy of the first excitation manifold for finite distance separation d between the QEs. We rewrite Eq. (7) in the dressed basis [Eq. (A2)]

$$\begin{aligned} \hat{\sigma}_1^+ &= \hat{\sigma}^+ \otimes \mathbb{1}, \\ &= |e\rangle\langle g| \otimes (|e\rangle\langle e| + |g\rangle\langle g|), \\ &= |e,e\rangle\langle g,e| + |e,g\rangle\langle g,g|, \\ &= \frac{1}{\sqrt{2}}(|X\rangle\langle +| + |X\rangle\langle -| + |+\rangle\langle G| - |-\rangle\langle G|), \\ \hat{\sigma}_2^+ &= \frac{1}{\sqrt{2}}(|X\rangle\langle +| - |X\rangle\langle -| + |+\rangle\langle G| + |-\rangle\langle G|), \end{aligned} \tag{A4}$$

where $|e,g\rangle = 1/\sqrt{2}(|+\rangle - |-\rangle)$ and $|g,e\rangle = 1/\sqrt{2}(|+\rangle + |-\rangle)$. Then, the SUPER terms in Eq. (7) $(\hat{\sigma}_1^+ e^{i\vartheta} + \hat{\sigma}_2^+)$ can be written as follows:

$$\begin{aligned} \hat{\sigma}_1^+ e^{i\vartheta} + \hat{\sigma}_2^+ = &\frac{e^{i\vartheta}}{\sqrt{2}}(|X\rangle\langle +| + |X\rangle\langle -| + |+\rangle\langle G| - |-\rangle\langle G|) \\ &+ \frac{1}{\sqrt{2}}(|X\rangle\langle +| - |X\rangle\langle -| + |+\rangle\langle G| + |-\rangle\langle G|). \end{aligned} \tag{A5}$$

Choosing $\vartheta = 0$ results in

$$\hat{\sigma}_1^+ + \hat{\sigma}_2^+ = \sqrt{2}(|X\rangle\langle +| + |+\rangle\langle G|). \tag{A6}$$

In this case, the SUPER terms in the dressed-states picture can be written as the following Hamiltonian:

$$\begin{aligned} \hat{\tilde{H}}_{\rm SUPER} = &-2\frac{\tilde{\Omega}_{\rm S}^1(t)}{2}(|X\rangle\langle +| + |+\rangle\langle G| + \text{H.c.}) - 2 \\ &\times \frac{\tilde{\Omega}_{\rm S}^2(t-\tau)}{2}\big((|X\rangle\langle +|+|+\rangle\langle G|)e^{i(\Delta_1-\Delta_2)t} + \text{H.c.}\big), \end{aligned} \tag{A7}$$

where $\tilde{\Omega}_{\rm S}^i(t) = \Omega_{\rm S}^i(t)/\sqrt{2}$. For $\vartheta = 0$, $\hat{\tilde{H}}_{\rm SUPER}$ couples only to the symmetric $|+\rangle$ branch. Similarly, $\vartheta = \pi$ leads to the SUPER pulses only coupling to the antisymmetric $|-\rangle$ branch. For the cavity Hamiltonian $\hat{H}_{\rm C}$ in Eq. (6), the same logic will remain applicable. For instance, the choice $\phi_1 = 0 = \phi_2$ leads to the mode only coupling to the $|+\rangle$ branch and, in contrast, for $\phi_1 = 0$ and $\phi_2 = \pi/2$ the cavity mode couples equally to branches $|+\rangle$ and $|-\rangle$ as shown below for the interaction part of $\hat{H}_{\rm C}$:

$$\begin{aligned} g\big(\hat{\sigma}_1^+ + \hat{\sigma}_2^+ e^{i\pi/2}\big)\hat{a} + \text{H.c.} = &\frac{1}{\sqrt{2}}(\tilde{g}(|X\rangle\langle +| + |+\rangle\langle G|) + \tilde{g}^* \\ &\times (|X\rangle\langle -| - |-\rangle\langle G|))\hat{a} + \text{H.c.}. \end{aligned} \tag{A8}$$

The coupling constant $g \to \tilde{g} = g(1+i)$ is now complex. The Hamiltonian in Eq. (7) in the dressed-state picture takes on the general form:

$$\begin{aligned} \hat{H}_{\rm DSP}(t) = &\sum_{j\in\{G,\pm,X\}} E_j|j\rangle\langle j| - \Delta_1\hat{a}^\dagger\hat{a} \\ &+ \frac{g}{\sqrt{2}}\sum_{j\in\{\pm\}}(\hat{a}(e^{i\phi_1}(|X\rangle\langle j| + \Xi(j)|j\rangle\langle G|) \\ &+ e^{i\phi_2}(\Xi(j)|X\rangle\langle j| + |j\rangle\langle G|)) + \text{H.c.}) \end{aligned}$$

$$
\begin{aligned}
&- \frac{\tilde{\Omega}_S^1(t)}{2} \sum_{j\in\{\pm\}} (e^{i\vartheta}(|X\rangle\langle j| + \Xi(j)|j\rangle\langle G|) \\
&+ (\Xi(j)|X\rangle\langle j| + |j\rangle\langle G|) + \text{H.c.}) \\
&- \frac{\tilde{\Omega}_S^2(t-\tau)}{2} \sum_{j\in\{\pm\}} \Big(e^{i(\Delta_1-\Delta_2)t}(e^{i\vartheta}(|X\rangle\langle j| \\
&+ \Xi(j)|j\rangle\langle G|) + (\Xi(j)|X\rangle\langle j| + |j\rangle\langle G|)) + \text{H.c.}\Big),
\end{aligned} \tag{A9}
$$

where $\Xi(\pm) = \pm 1$. The collective decay rates $\Gamma_\pm = \Gamma \pm \Gamma_{12}$ can be obtained simply by rewriting the Liouvillian superoperator in terms of the dressed states [121]. For $\Gamma_{12} > 0$, the $|+\rangle$ branch is the superradiant and the $|-\rangle$ branch is the subradiant decay channel. The branches switch roles when $\Gamma_{12} < 0$.

Considering Eq. (A7), we recognize that the two identical SUPER pulses in $\hat{H}(t)$, acting on the two QEs separately, interact in the dressed-states picture in a way such that the beatlike interference of the two Gaussian pulses spreads over the entire $|+\rangle$ branch: $|X\rangle\langle +| + |+\rangle\langle G|$. Depending on the optimized parameters discussed in Sec. III C, we can address $|+\rangle$ or $|X\rangle$ directly. For $\vartheta = \pi$, this is true for the $|-\rangle$ branch. A more detailed discussion is given in Appendix B.

APPENDIX B: THE INFLUENCE OF PHASES IN POPULATING EXCITED STATES OF COUPLED QUANTUM EMITTERS

As discussed in Sec. III D, the Bloch representation is very useful to visualize the population dynamics of the system with the SUPER scheme. However, this representation does not provide complete information about the influence of ϑ on the state populations $P_\pm$ and $P_{e,e}$ with the relative phase ϑ. Here, we specifically plot the populations $P_\pm(t, \vartheta)$ [panels (a)–(d)] and $P_{e,e}(t, \vartheta)$ [panels (e) and (f)] in Figs. 9 and 10, respectively, explicitly pointing out the dependence on ϑ and the temporal evolution. In panels (a), (c), and (e), the time evolutions during the SUPER excitation is displayed, whereas panels (b), (d), and (f) present the corresponding long-time evolutions of the system. Figure 9 shows the variations for $d = 0.01\lambda$ and with chosen pulse areas $\alpha_1 = 68.25\pi$ and $\alpha_2 = 59.05\pi$ ($|+\rangle$ is the target state). The horizontal lines indicate the corresponding Bloch-sphere dynamics that are denoted by red dashed cut at $\vartheta = 0$ [see Fig. 6(a)], orange dashed cut at $\vartheta = \pm\pi/2$ [for Fig. 6(b)], and yellow/black dashed cut at $\vartheta = \pm\pi$ [in Fig. 6(c)]. Similarly in Fig. 10, where we use $\alpha_1 = 51.74\pi$ and $\alpha_2 = 70.48\pi$ at $d = 0.1\lambda$ ($|X\rangle$ is the target state). The corresponding Bloch dynamics are presented in Figs. 6(d)–6(f).

Considering the case of the target state $|+\rangle$, Fig. 9(a) clearly shows that the choice of ϑ is crucial. This is expected, since ϑ dictates the values of the mixture weights $h_{i,j}$ in Eq. (21). The off-diagonal $h_{i,j}$ mediate the SUPER mechanism for the transition $|j\rangle \to |i\rangle$. The SUPER parameters are optimized for the ideal case of $\vartheta = 0$, i.e., $h_{X,+} = h_{+,G} = -\tilde{\Omega}_S(t) \neq 0$ and $h_{X,-} = h_{-,G} = 0$ (Table II). The choice $\vartheta \neq 0$ allows the excitation to penetrate into the $|-\rangle$ branch. This reduces the final population significantly. One would expect

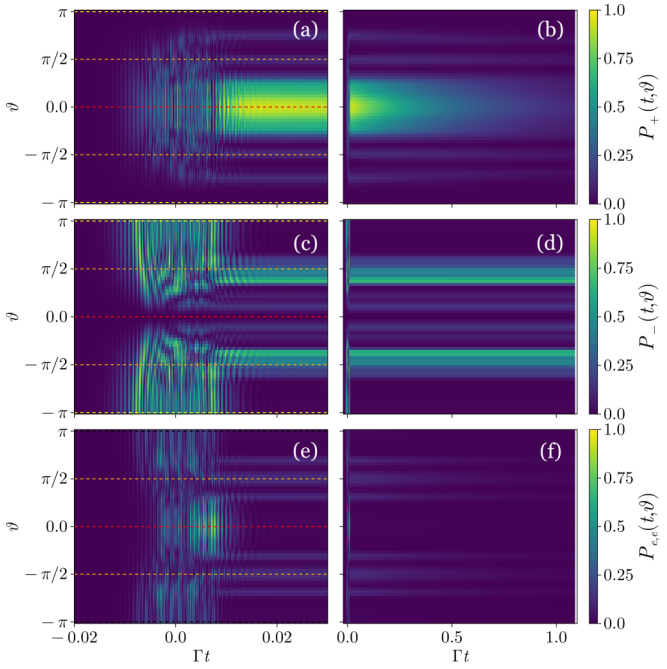


FIG. 9. The populations $P_+(t, \vartheta)$ [panels (a) and (b)], $P_-(t, \vartheta)$ [panels (c) and (d)], and $P_{e,e}(t, \vartheta)$ [panels (e) and (f)] with $\vartheta \in (-\pi, \pi]$ are shown when $d = 0.01\lambda$. Red, orange, and yellow/black horizontal dashed lines in panels (a), (c), and (e) correspond to $\vartheta = 0, \pm\pi/2, \pm\pi$, indicating the dynamical trajectories in the Bloch-sphere as shown in Figs. 6(a), 6(b), and 6(c), respectively.

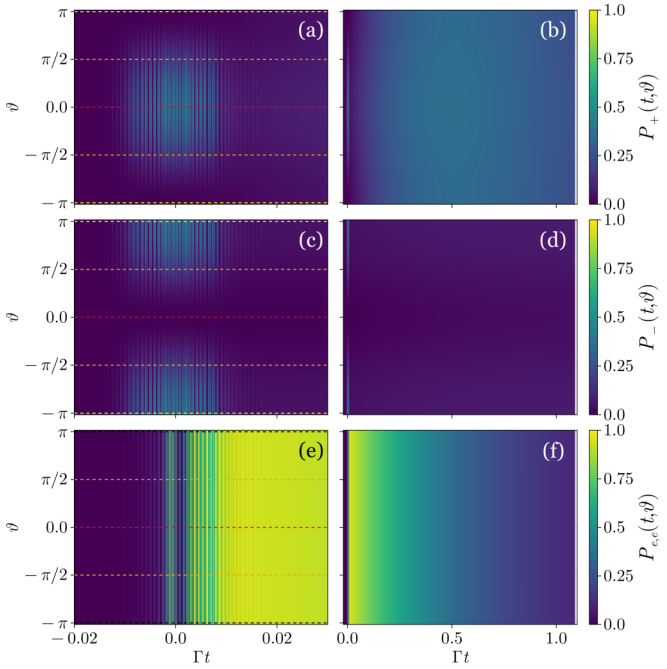


FIG. 10. The populations $P_+(t, \vartheta)$ [panels (a) and (b)], $P_-(t, \vartheta)$ [panels (c) and (d)], and $P_{e,e}(t, \vartheta)$ [panels (e) and (f)] with $\vartheta \in (-\pi, \pi]$ are shown for $d = 0.1\lambda$. Red, orange, and yellow/black horizontal dashed lines in panels (a), (c), and (e) correspond to $\vartheta = 0, \pm\pi/2, \pm\pi$, representing the dynamical trajectories in the Bloch-sphere as shown in Figs. 6(d), 6(e), and 6(f), respectively.

a small, even no, increase of the final population in $|-\rangle$ for $\vartheta \to \pm\pi$, since the collective fine-structure splitting Ω_{12} implies $E_+ \gg E_-$. This can be observed. The final population of $|X\rangle$ remains small in this case.

Focusing now on the efficient population of $|X\rangle$ in Fig. 10(c), an interesting behavior emerges. We find that the choice of ϑ does not influence the outcome of the final population in $|X\rangle$ at all, even though the mixture weights $h_{i,j} \neq 0$ allow contributions of both, the $|+\rangle$ and $|-\rangle$ branch. One might naively expect this to always apply to the $|X\rangle$ state preparation, regardless of the interemitter separation d, because the final energy E_X remains the same and the SUPER pulses constructively interfere with each other. However, for example, while we can find optimized parameters to efficiently populate $|X\rangle$ with $\vartheta = \pi$ (using the $|-\rangle$ branch) at $d = 0.01\lambda$ (not shown in this manuscript), we observe close-to-zero inversions $\forall |j\rangle \in \{|\pm\rangle, |X\rangle\}$ if $0 < |\vartheta| < \pi$. This implies that the SUPER pulse interferences are nontrivial and are greatly influenced by the mixture weights $h_{i,j}$ ($h^*_{i,j}$) as well as Ω_{12}.

[1] M. Reitz, C. Sommer, and C. Genes, Cooperative quantum phenomena in light-matter platforms, PRX Quantum **3**, 010201 (2022).

[2] J. Ruostekoski, Cooperative quantum-optical planar arrays of atoms, Phys. Rev. A **108**, 030101 (2023).

[3] R. H. Dicke, Coherence in spontaneous radiation processes, Phys. Rev. **93**, 99 (1954).

[4] M. Gross and S. Haroche, Superradiance: An essay on the theory of collective spontaneous emission, Phys. Rep. **93**, 301 (1982).

[5] R. G. DeVoe and R. G. Brewer, Observation of superradiant and subradiant spontaneous emission of two trapped ions, Phys. Rev. Lett. **76**, 2049 (1996).

[6] C. Hettich, C. Schmitt, J. Zitzmann, S. Kühn, I. Gerhardt, and V. Sandoghdar, Nanometer resolution and coherent optical dipole coupling of two individual molecules, Science **298**, 385 (2002).

[7] H. Zoubi and H. Ritsch, Metastability and directional emission characteristics of excitons in 1D optical lattices, Europhys. Lett. **90**, 23001 (2010).

[8] K. D. B. Higgins, S. C. Benjamin, T. M. Stace, G. J. Milburn, B. W. Lovett, and E. M. Gauger, Superabsorption of light via quantum engineering, Nat. Commun. **5**, 4705 (2014).

[9] A. Asenjo-Garcia, M. Moreno-Cardoner, A. Albrecht, H. J. Kimble, and D. E. Chang, Exponential improvement in photon storage fidelities using subradiance and "selective radiance" in atomic arrays, Phys. Rev. X **7**, 031024 (2017).

[10] P.-O. Guimond, A. Grankin, D. V. Vasilyev, B. Vermersch, and P. Zoller, Subradiant Bell states in distant atomic arrays, Phys. Rev. Lett. **122**, 093601 (2019).

[11] J. Kim, D. Yang, S. hoon Oh, and K. An, Coherent single-atom superradiance, Science **359**, 662 (2018).

[12] J. Rui, D. Wei, A. Rubio-Abadal, S. Hollerith, J. Zeiher, D. M. Stamper-Kurn, C. Gross, and I. Bloch, A subradiant optical mirror formed by a single structured atomic layer, Nature (London) **583**, 369 (2020).

[13] X. H. H. Zhang, D. Malz, and P. Rabl, Unraveling superradiance: Entanglement and mutual information in collective decay, Phys. Rev. Lett. **135**, 033602 (2025).

[14] J. A. Mlynek, A. A. Abdumalikov, C. Eichler, and A. Wallraff, Observation of Dicke superradiance for two artificial atoms in a cavity with high decay rate, Nat. Commun. **5**, 5186 (2014).

[15] Z. X. Koong, M. Cygorek, E. Scerri, T. S. Santana, S. I. Park, J. D. Song, E. M. Gauger, and B. D. Gerardot, Coherence in cooperative photon emission from indistinguishable quantum emitters, Sci. Adv. **8**, eabm8171 (2022).

[16] M. Zanner, T. Orell, C. M. F. Schneider, R. Albert, S. Oleschko, M. L. Juan, M. Silveri, and G. Kirchmair, Coherent control of a multi-qubit dark state in waveguide quantum electrodynamics, Nat. Phys. **18**, 538 (2022).

[17] J. B. Trebbia, Q. Deplano, P. Tamarat, and B. Lounis, Tailoring the superradiant and subradiant nature of two coherently coupled quantum emitters, Nat. Commun. **13**, 2962 (2022).

[18] A. Tiranov, V. Angelopoulou, C. J. van Diepen, B. Schrinski, O. A. D. Sandberg, Y. Wang, L. Midolo, S. Scholz, A. D. Wieck, A. Ludwig, A. S. Sørensen, and P. Lodahl, Collective super- and subradiant dynamics between distant optical quantum emitters, Science **379**, 389 (2023).

[19] C. M. Lange, E. Daggett, V. Walther, L. Huang, and J. D. Hood, Superradiant and subradiant states in lifetime-limited organic molecules through laser-induced tuning, Nat. Phys. **20**, 836 (2024).

[20] M. Scheibner, T. Schmidt, L. Worschech, A. Forchel, G. Bacher, T. Passow, and D. Hommel, Superradiance of quantum dots, Nat. Phys. **3**, 106 (2007).

[21] W. Guerin, M. O. Araújo, and R. Kaiser, Subradiance in a large cloud of cold atoms, Phys. Rev. Lett. **116**, 083601 (2016).

[22] G. Ferioli, A. Glicenstein, L. Henriet, I. Ferrier-Barbut, and A. Browaeys, Storage and release of subradiant excitations in a dense atomic cloud, Phys. Rev. X **11**, 021031 (2021).

[23] C. Hotter, L. Ostermann, and H. Ritsch, Cavity sub- and superradiance for transversely driven atomic ensembles, Phys. Rev. Res. **5**, 013056 (2023).

[24] M. Fasser, L. Ostermann, H. Ritsch, and C. Hotter, Subradiance and superradiant long-range excitation transport among quantum emitter ensembles in a waveguide, Opt. Quantum **2**, 397 (2024).

[25] J. G. Bohnet, Z. Chen, J. M. Weiner, D. Meiser, M. J. Holland, and J. K. Thompson, A steady-state superradiant laser with less than one intracavity photon, Nature (London) **484**, 78 (2012).

[26] G. Facchinetti, S. D. Jenkins, and J. Ruostekoski, Storing light with subradiant correlations in arrays of atoms, Phys. Rev. Lett. **117**, 243601 (2016).

[27] R. Holzinger, D. Plankensteiner, L. Ostermann, and H. Ritsch, Nanoscale coherent light source, Phys. Rev. Lett. **124**, 253603 (2020).

[28] F. Mattiotti, W. M. Brown, N. Piovella, S. Olivares, E. M. Gauger, and G. L. Celardo, Bio-inspired natural sunlight-pumped lasers, New J. Phys. **23**, 103015 (2021).

[29] N. Werren, W. Brown, and E. M. Gauger, Light harvesting enhanced by quantum ratchet states, PRX Energy **2**, 013002 (2023).

[30] A. Burgess, M. C. Waller, E. M. Gauger, and R. Bennett, Engineering dipole-dipole couplings for enhanced cooperative light-matter interactions, Phys. Rev. Lett. **134**, 113602 (2025).

[31] J. L. O'Brien, A. Furusawa, and J. Vučković, Photonic quantum technologies, Nat. Photon. **3**, 687 (2009).

[32] K. Hammerer, A. S. Sørensen, and E. S. Polzik, Quantum interface between light and atomic ensembles, Rev. Mod. Phys. **82**, 1041 (2010).

[33] A. C. Santos, A. Cidrim, C. J. Villas-Boas, R. Kaiser, and R. Bachelard, Generating long-lived entangled states with free-space collective spontaneous emission, Phys. Rev. A **105**, 053715 (2022).

[34] A. C. Santos and R. Bachelard, Generation of maximally entangled long-lived states with giant atoms in a waveguide, Phys. Rev. Lett. **130**, 053601 (2023).

[35] L. Ostermann, H. Ritsch, and C. Genes, Protected state enhanced quantum metrology with interacting two-level ensembles, Phys. Rev. Lett. **111**, 123601 (2013).

[36] L. Pezzè, A. Smerzi, M. K. Oberthaler, R. Schmied, and P. Treutlein, Quantum metrology with nonclassical states of atomic ensembles, Rev. Mod. Phys. **90**, 035005 (2018).

[37] J. Ye and P. Zoller, Essay: Quantum sensing with atomic, molecular, and optical platforms for fundamental physics, Phys. Rev. Lett. **132**, 190001 (2024).

[38] F. Jahnke, C. Gies, M. Aßmann, M. Bayer, H. A. M. Leymann, A. Foerster, J. Wiersig, C. Schneider, M. Kamp, and S. Höfling, Giant photon bunching, superradiant pulse emission and excitation trapping in quantum-dot nanolasers, Nat. Commun. **7**, 11540 (2016).

[39] E. A. Bohr, S. L. Kristensen, C. Hotter, S. A. Schäffer, J. Robinson-Tait, J. W. Thomsen, T. Zelevinsky, H. Ritsch, and J. H. Müller, Collectively enhanced Ramsey readout by cavity sub- to superradiant transition, Nat. Commun. **15**, 1084 (2024).

[40] A. Juan-Delgado, R. Esteban, A. Nodar, J.-B. Trebbia, B. Lounis, and J. Aizpurua, Tailoring the statistics of light emitted from two interacting quantum emitters, Phys. Rev. Res. **6**, 023207 (2024).

[41] F. B. Zhelezko, I. M. Gulis, B. Lounis, and M. Orrit, Spectroscopic characteristics of single dibenzanthanthrene molecules isolated in a low-temperature naphthalene matrix, J. Appl. Spectrosc. **66**, 344 (1999).

[42] P. Laferrière, E. Yeung, L. Giner, S. Haffouz, J. Lapointe, G. C. Aers, P. J. Poole, R. L. Williams, and D. Dalacu, Multiplexed single-photon source based on multiple quantum dots embedded within a single nanowire, Nano Lett. **20**, 3688 (2020).

[43] D. Huber, M. Reindl, S. F. Covre da Silva, C. Schimpf, J. Martín-Sánchez, H. Huang, G. Piredda, J. Edlinger, A. Rastelli, and R. Trotta, Strain-tunable GaAs quantum dot: A nearly dephasing-free source of entangled photon pairs on demand, Phys. Rev. Lett. **121**, 033902 (2018).

[44] X.-L. Chu, V. Angelopoulou, P. Lodahl, and N. Rotenberg, Subradiant states for two imperfect quantum emitters coupled by a nanophotonic waveguide, Phys. Rev. A **106**, 053702 (2022).

[45] P. Lodahl, S. Mahmoodian, and S. Stobbe, Interfacing single photons and single quantum dots with photonic nanostructures, Rev. Mod. Phys. **87**, 347 (2015).

[46] C. J. van Diepen, V. Angelopoulou, O. A. D. Sandberg, A. Tiranov, Y. Wang, S. Scholz, A. Ludwig, A. Søndberg Sørensen, and P. Lodahl, Resonant energy transfer and collectively driven emitters in waveguide QED, Phys. Rev. Res. **7**, 033169 (2025).

[47] K.-Y. Kim, J. H. Lee, W. B. Jeon, D. H. Park, S. I. Park, J. D. Song, C. Lee, and J.-H. Kim, Cavity-mediated collective emission from steady-state subradiance, Nat. Commun. **16**, 6346 (2025).

[48] D. Plankensteiner, L. Ostermann, H. Ritsch, and C. Genes, Selective protected state preparation of coupled dissipative quantum emitters, Sci. Rep. **5**, 16231 (2015).

[49] H. H. Jen, M.-S. Chang, and Y.-C. Chen, Cooperative single-photon subradiant states, Phys. Rev. A **94**, 013803 (2016).

[50] T. K. Bracht, M. Cosacchi, T. Seidelmann, M. Cygorek, A. Vagov, V. M. Axt, T. Heindel, and D. E. Reiter, Swing-up of quantum emitter population using detuned pulses, PRX Quantum **2**, 040354 (2021).

[51] Y. Karli, F. Kappe, V. Remesh, T. K. Bracht, J. Münzberg, S. Covre da Silva, T. Seidelmann, V. M. Axt, A. Rastelli, D. E. Reiter, and G. Weihs, Super scheme in action: Experimental demonstration of red-detuned excitation of a quantum emitter, Nano Lett. **22**, 6567 (2022).

[52] C. G. Torun, M. Gökçe, T. K. Bracht, M. I. Monsalve, S. Benbouabdellah, Özgün Ozan Nacitarhan, M. E. Stucki, M. L. Markham, G. Pieplow, T. Pregnolato, J. H. D. Munns, D. E. Reiter, and T. Schröder, Super and subpicosecond coherent control of an optical qubit in a tin-vacancy color center in diamond, arXiv:2312.05246.

[53] K. Boos, F. Sbresny, S. K. Kim, M. Kremser, H. Riedl, F. W. Bopp, W. Rauhaus, B. Scaparra, K. D. Jöns, J. J. Finley, K. Müller, and L. Hanschke, Coherent swing-up excitation for semiconductor quantum dots, Adv. Quantum Technol. **7**, 2300359 (2024).

[54] R. Joos, S. Bauer, C. Rupp, S. Kolatschek, W. Fischer, C. Nawrath, P. Vijayan, R. Sittig, M. Jetter, S. L. Portalupi, and P. Michler, Coherently and incoherently pumped telecom C-band single-photon source with high brightness and indistinguishability, Nano Lett. **24**, 8626 (2024).

[55] T. K. Bracht, T. Seidelmann, T. Kuhn, V. M. Axt, and D. E. Reiter, Phonon wave packet emission during state preparation of a semiconductor quantum dot using different schemes, Phys. Status Solidi B **259**, 2100649 (2022).

[56] N. Heinisch, N. Köcher, D. Bauch, and S. Schumacher, Swing-up dynamics in quantum emitter cavity systems: Near ideal single photons and entangled photon pairs, Phys. Rev. Res. **6**, L012017 (2024).

[57] T. K. Bracht, M. Cygorek, T. Seidelmann, V. M. Axt, and D. E. Reiter, Temperature-independent almost perfect photon entanglement from quantum dots via the super scheme, Optica Quantum **1**, 103 (2023).

[58] T. K. Bracht, T. Seidelmann, Y. Karli, F. Kappe, V. Remesh, G. Weihs, V. M. Axt, and D. E. Reiter, Dressed-state analysis of two-color excitation schemes, Phys. Rev. B **107**, 035425 (2023).

[59] L. Vannucci and N. Gregersen, Super excitation of quantum emitters is a multi-photon process, Opt. Express **32**, 35381 (2024).

[60] Q. W. Richter, J. M. Kaspari, T. K. Bracht, L. Yatsenko, V. M. Axt, A. Rauschenbeutel, and D. E. Reiter, Few-photon super: Quantum emitter inversion via two off-resonant photon modes, Phys. Rev. Res. **7**, 013079 (2025).

[61] S. Haroche and D. Kleppner, Cavity quantum electrodynamics, Phys. Today **42**(1), 24 (1989).

[62] Z. Ficek and R. Tanaś, Entangled states and collective nonclassical effects in two-atom systems, Phys. Rep. **372**, 369 (2002).

[63] N. J. Hestand and F. C. Spano, Expanded theory of H- and J-molecular aggregates: The effects of vibronic coupling and intermolecular charge transfer, Chem. Rev. **118**, 7069 (2018).

[64] K. Srinivasan and O. Painter, Mode coupling and cavity–quantum-dot interactions in a fiber-coupled microdisk cavity, Phys. Rev. A **75**, 023814 (2007).

[65] M. Cosacchi, J. Wiercinski, T. Seidelmann, M. Cygorek, A. Vagov, D. E. Reiter, and V. M. Axt, On-demand generation of higher-order Fock states in quantum-dot–cavity systems, Phys. Rev. Res. **2**, 033489 (2020).

[66] V. May and O. Kühn, *Charge and Energy Transfer Dynamics in Molecular Systems* (Wiley-VCH, Weinheim, 2004).

[67] P. Rebentrost, M. Mohseni, I. Kassal, S. Lloyd, and A. Aspuru-Guzik, Environment-assisted quantum transport, New J. Phys. **11**, 033003 (2009).

[68] A. Pal, R. Holzinger, M. Moreno-Cardoner, and H. Ritsch, Efficient excitation transfer in an LH2-inspired nanoscale stacked ring geometry, New J. Phys. **27**, 094101 (2025).

[69] N. Lambert, Y.-N. Chen, Y.-C. Cheng, C.-M. Li, G.-Y. Chen, and F. Nori, Quantum biology, Nat. Phys. **9**, 10 (2013).

[70] R. J. Cogdell, A. Gall, and J. Köhler, The architecture and function of the light-harvesting apparatus of purple bacteria: From single molecules to *in vivo* membranes, Q. Rev. Biophys. **39**, 227 (2006).

[71] R. Monshouwer, M. Abrahamsson, F. van Mourik, and R. van Grondelle, Superradiance and exciton delocalization in bacterial photosynthetic light-harvesting systems, J. Phys. Chem. B **101**, 7241 (1997).

[72] D. Ferrari, G. L. Celardo, G. P. Berman, R. T. Sayre, and F. Borgonovi, Quantum biological switch based on superradiance transitions, J. Phys. Chem. C **118**, 20 (2014).

[73] H. Gotfredsen, J.-R. Deng, J. M. Van Raden, M. Righetto, J. Hergenhahn, M. Clarke, A. Bellamy-Carter, J. Hart, J. O'Shea, T. D. W. Claridge, F. Duarte, A. Saywell, L. M. Herz, and H. L. Anderson, Bending a photonic wire into a ring, Nat. Chem. **14**, 1436 (2022).

[74] F. C. Spano and S. Mukamel, Superradiance in molecular aggregates, J. Chem. Phys. **91**, 683 (1989).

[75] J. Grad, G. Hernandez, and S. Mukamel, Radiative decay and energy transfer in molecular aggregates: The role of intermolecular dephasing, Phys. Rev. A **37**, 3835 (1988).

[76] E. Gauger, Bio-inspired quantum energy harvesting with collective light-matter effects, in *Quantum Effects and Measurement Techniques in Biology and Biophotonics*, edited by C. Aiello, S. V. Polyakov, and P. Derr (International Society for Optics and Photonics, SPIE, San Francisco, California, 2024), Vol. 12863, p. 1286308.

[77] M. Moreno-Cardoner, R. Holzinger, and H. Ritsch, Efficient nano-photonic antennas based on dark states in quantum emitter rings, Opt. Express **30**, 10779 (2022).

[78] R. Holzinger, J. S. Peter, S. Ostermann, H. Ritsch, and S. Yelin, Harnessing quantum emitter rings for efficient energy transport and trapping, Optica Quantum **2**, 57 (2024).

[79] F. Bloch, Nuclear induction, Phys. Rev. **70**, 460 (1946).

[80] I. M. Mirza and S. J. van Enk, Single-photon time-dependent spectra in quantum optomechanics, Phys. Rev. A **90**, 043831 (2014).

[81] R. Filip and L. Mišta, Detecting quantum states with a positive Wigner function beyond mixtures of Gaussian states, Phys. Rev. Lett. **106**, 200401 (2011).

[82] M. Ježek, I. Straka, M. Mičuda, M. Dušek, J. Fiurášek, and R. Filip, Experimental test of the quantum non-Gaussian character of a heralded single-photon state, Phys. Rev. Lett. **107**, 213602 (2011).

[83] I. Straka, A. Predojević, T. Huber, L. Lachman, L. Butschek, M. Miková, M. Mičuda, G. S. Solomon, G. Weihs, M. Ježek, and R. Filip, Quantum non-Gaussian depth of single-photon states, Phys. Rev. Lett. **113**, 223603 (2014).

[84] M. Gurioli, Z. Wang, A. Rastelli, T. Kuroda, and S. Sanguinetti, Droplet epitaxy of semiconductor nanostructures for quantum photonic devices, Nat. Mater. **18**, 799 (2019).

[85] D. Dalacu, P. J. Poole, and R. L. Williams, Tailoring the geometry of bottom-up nanowires: Application to high efficiency single photon sources, Nanomaterials **11**, 1201 (2021).

[86] P. Laferrière, E. Yeung, I. Miron, D. B. Northeast, S. Haffouz, J. Lapointe, M. Korkusinski, P. J. Poole, R. L. Williams, and D. Dalacu, Unity yield of deterministically positioned quantum dot single photon sources, Sci. Rep. **12**, 6376 (2022).

[87] A. W. Schell, G. Kewes, T. Schröder, J. Wolters, T. Aichele, and O. Benson, A scanning probe-based pick-and-place procedure for assembly of integrated quantum optical hybrid devices, Rev. Sci. Instrum. **82**, 073709 (2011).

[88] J. Shamsi, A. S. Urban, M. Imran, L. De Trizio, and L. Manna, Metal halide perovskite nanocrystals: Synthesis, post-synthesis modifications, and their optical properties, Chem. Rev. **119**, 3296 (2019).

[89] M. Fu, P. Tamarat, H. Huang, J. Even, A. L. Rogach, and B. Lounis, Neutral and charged exciton fine structure in single lead halide perovskite nanocrystals revealed by magneto-optical spectroscopy, Nano Lett. **17**, 2895 (2017).

[90] A. K. Adamczyk, T. A. P. M. Huijben, M. Sison, A. Di Luca, G. Chiarelli, S. Vanni, S. Brasselet, K. I. Mortensen, F. D. Stefani, M. Pilo-Pais, and G. P. Acuna, DNA self-assembly of single molecules with deterministic position and orientation, ACS Nano **16**, 16924 (2022).

[91] A. Gopinath, C. Thachuk, A. Mitskovets, H. A. Atwater, D. Kirkpatrick, and P. W. K. Rothemund, Absolute and arbitrary orientation of single-molecule shapes, Science **371**, eabd6179 (2021).

[92] G. Haider, K. Sampathkumar, T. Verhagen, L. Nádvorník, F. J. Sonia, V. Valeš, J. Sýkora, P. Kapusta, P. Němec, M. Hof, O. Frank, Y.-F. Chen, J. Vejpravová, and M. Kalbáč, Superradiant emission from coherent excitons in van der Waals heterostructures, Adv. Funct. Mater. **31**, 2102196 (2021).

[93] J. Kumlin, A. Srivastava, and T. Pohl, Superradiance of strongly interacting dipolar excitons in moiré quantum materials, Phys. Rev. Lett. **134**, 126901 (2025).

[94] C. Chakraborty, N. Vamivakas, and D. Englund, Advances in quantum light emission from 2D materials, Nanophotonics **8**, 2017 (2019).

[95] D. Hallett, J. Wiercinski, L. Hallacy, S. Sheldon, R. Dost, N. Martin, A. Fenzl, I. Farrer, A. Verma, M. Cygorek, E. M. Gauger, M. S. Skolnick, and L. R. Wilson, Controlling coherence between waveguide-coupled quantum dots, Phys. Rev. Appl. (2026).

[96] J. Nobakht, A. Pscherer, J. Renger, S. Götzinger, and V. Sandoghdar, Hybridization of molecules via a common photonic mode, Proc. Natl. Acad. Sci. USA **122**, e2505161122 (2025).

[97] J.-H. Kim, S. Aghaeimeibodi, C. J. K. Richardson, R. P. Leavitt, and E. Waks, Super-radiant emission from quantum dots in a nanophotonic waveguide, Nano Lett. **18**, 4734 (2018).

[98] B. Gerardot, S. Seidl, P. Dalgarno, R. J. Warburton, D. Granados, J. Garcia, K. Kowalik, O. Krebs, K. Karrai, A. Badolato, *et al.*, Manipulating exciton fine structure in quantum dots with a lateral electric field, Appl. Phys. Lett. **90**, 041101 (2007).

[99] A. Bennett, M. Pooley, R. Stevenson, M. Ward, R. Patel, A. B. de La Giroday, N. Sköld, I. Farrer, C. Nicoll, D. Ritchie, *et al.*, Electric-field-induced coherent coupling of the exciton states in a single quantum dot, Nat. Phys. **6**, 947 (2010).

[100] A. Rastelli *et al.*, Controlling quantum dot emission by integration of semiconductor nanomembranes onto piezoelectric actuators, Phys. Status Solidi B **249**, 687 (2012).

[101] A. W. Elshaari, E. Büyüközer, I. E. Zadeh, T. Lettner, P. Zhao, E. Schöll, S. Gyger, M. E. Reimer, D. Dalacu, P. J. Poole, K. D. Jöns, and V. Zwiller, Strain-tunable quantum integrated photonics, Nano Lett. **18**, 7969 (2018).

[102] Z.-X. Koong, G. Ballesteros-Garcia, R. Proux, D. Dalacu, P. J. Poole, and B. D. Gerardot, Multiplexed single photons from deterministically positioned nanowire quantum dots, Phys. Rev. Appl. **14**, 034011 (2020).

[103] J. Phoenix, M. Korkusinski, D. Dalacu, P. J. Poole, P. Zawadzki, S. Studenikin, R. L. Williams, A. S. Sachrajda, and L. Gaudreau, Magnetic tuning of tunnel coupling between InAsP double quantum dots in InP nanowires, Sci. Rep. **12**, 5100 (2022).

[104] J. Q. Grim, A. S. Bracker, M. Zalalutdinov, S. G. Carter, A. C. Kozen, M. Kim, C. S. Kim, J. T. Mlack, M. Yakes, B. Lee, and D. Gammon, Scalable in operando strain tuning in nanophotonic waveguides enabling three-quantum-dot superradiance, Nat. Mater. **18**, 963 (2019).

[105] P. J. Leek, M. Baur, J. M. Fink, R. Bianchetti, L. Steffen, S. Filipp, and A. Wallraff, Cavity quantum electrodynamics with separate photon storage and qubit readout modes, Phys. Rev. Lett. **104**, 100504 (2010).

[106] D. Heinze, D. Breddermann, A. Zrenner, and S. Schumacher, A quantum dot single-photon source with on-the-fly all-optical polarization control and timed emission, Nat. Commun. **6**, 8473 (2015).

[107] N. O. Gjonbalaj, S. Ostermann, and S. F. Yelin, Modifying cooperative decay via disorder in atom arrays, Phys. Rev. A **109**, 013720 (2024).

[108] B. Olmos and I. Lesanovsky, Hybrid sub- and superradiant states in emitter arrays with quantized motion, Phys. Rev. Lett. **134**, 243602 (2025).

[109] B. Lounis and M. Orrit, Single-photon sources, Rep. Prog. Phys. **68**, 1129 (2005).

[110] P. Senellart, G. Solomon, and A. White, High-performance semiconductor quantum-dot single-photon sources, Nat. Nanotechnol. **12**, 1026 (2017).

[111] A. Reiserer, Colloquium: Cavity-enhanced quantum network nodes, Rev. Mod. Phys. **94**, 041003 (2022).

[112] K. Azuma, S. E. Economou, D. Elkouss, P. Hilaire, L. Jiang, H.-K. Lo, and I. Tzitrin, Quantum repeaters: From quantum networks to the quantum internet, Rev. Mod. Phys. **95**, 045006 (2023).

[113] C. Couteau, S. Barz, T. Durt, T. Gerrits, J. Huwer, R. Prevedel, J. Rarity, A. Shields, and G. Weihs, Applications of single photons to quantum communication and computing, Nat. Rev. Phys. **5**, 326 (2023).

[114] B. Lounis and W. E. Moerner, Single photons on demand from a single molecule at room temperature, Nature (London) **407**, 491 (2000).

[115] T. Heindel, J.-H. Kim, N. Gregersen, A. Rastelli, and S. Reitzenstein, Quantum dots for photonic quantum information technology, Adv. Opt. Photon. **15**, 613 (2023).

[116] S. Krämer, D. Plankensteiner, L. Ostermann, and H. Ritsch, Quantumoptics.jl: A Julia framework for simulating open quantum systems, Comput. Phys. Commun. **227**, 109 (2018).

[117] https://qojulia.github.io/CollectiveSpins.jl/.

[118] A. Mercurio, Y.-T. Huang, L.-X. Cai, Y.-N. Chen, V. Savona, and F. Nori, QuantumToolbox.jl: An efficient Julia framework for simulating open quantum systems, Quantum **9**, 1866 (2025).

[119] S. Danisch and J. Krumbiegel, Makie.jl: Flexible high-performance data visualization for Julia, J. Open Source Software **6**, 3349 (2021).

[120] J. Kerber, L. Ostermann, V. Remesh, H. Ritsch, and A. Pal, Selective preparation of collective states in coupled quantum emitters using the SUPER excitation scheme, Zenodo (2026), https://doi.org/10.5281/zenodo.18232292.

[121] L. Ostermann, Collective radiation of coupled atomic dipoles and the precise measurement of time, Ph.D. thesis, University of Innsbruck, 2016.